Article

Current Biology

Social play behavior is driven by glycine-dependent mechanisms

Graphical abstract

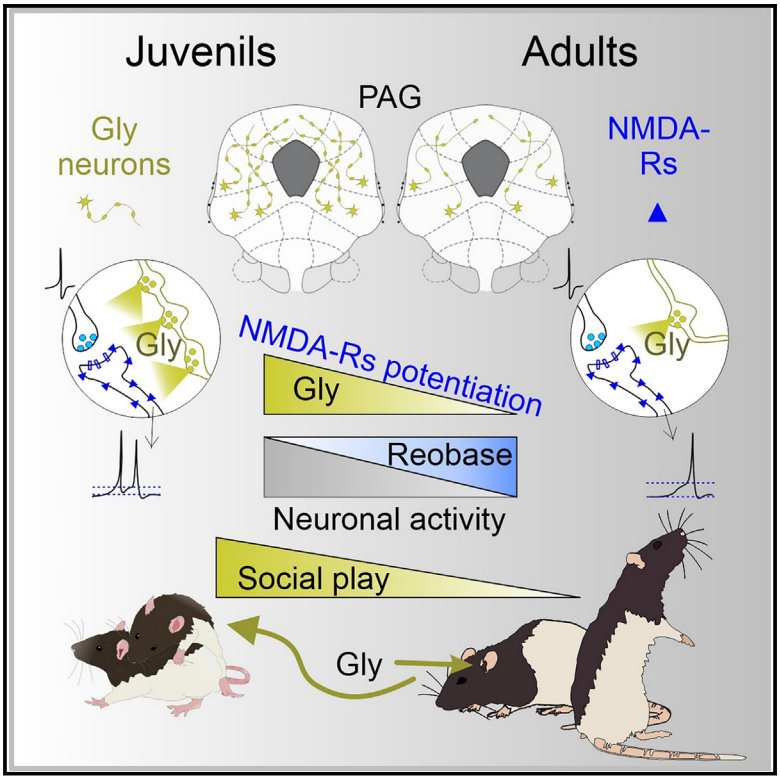

Authors

Anton Dvorzhak, Michael Brecht, Dietmar Schmitz

Correspondence

dietmar.schmitz@charite.de

In brief

Dvorzhak et al. show that the age-related decline in the social playfulness of rats depends in part on glycinergic synaptic transmission in the periaqueductal gray (PAG), a structure whose neuronal activity is required for social play. Glycine stimulates social play through NMDA receptors potentiation, which increases neuronal activity in the PAG.

Highlights

- Activity of periaqueductal gray (PAG) neurons is required for social play
- Neuronal activity and glycinergic neurotransmission in PAG decline with age
- Glycine stimulates social play through potentiation of NMDA receptors in PAG
- Age-related social play decrease is partially dependent on glycine decline in PAG

Dvorzhak et al., 2024, Current Biology *34*, 1–11
August 19, 2024
https://doi.org/10.1016/j.cub.2024.06.073

CellPress

Current Biology

CellPress
OPEN ACCESS

Article

Social play behavior is driven by glycine-dependent mechanisms

Anton Dvorzhak,[1] Michael Brecht,[2,3] and Dietmar Schmitz[1,2,3,4,5,6,7,*]

[1]Charité-Universitätsmedizin Berlin, Freie Universität Berlin and Humboldt-Universität zu Berlin, Neuroscience Research Center, 10117 Berlin, Germany
[2]Humboldt-Universität zu Berlin, Bernstein Center for Computational Neuroscience, Philippstr. 13, 10115 Berlin, Germany
[3]Charité-Universitätsmedizin Berlin, Freie Universität Berlin and Humboldt-Universität zu Berlin, NeuroCure Cluster of Excellence, 10117 Berlin, Germany
[4]German Center for Neurodegenerative Diseases (DZNE), 10117 Berlin, Germany
[5]Charité-Universitätsmedizin Berlin, Freie Universität Berlin and Humboldt-Universität zu Berlin, Einstein Center for Neuroscience, 10117 Berlin, Germany
[6]Max Delbrück Center for Molecular Medicine in the Helmholtz Association, Robert-Rössle-Straße 10, 13125 Berlin, Germany
[7]Lead contact
*Correspondence: dietmar.schmitz@charite.de
https://doi.org/10.1016/j.cub.2024.06.073

SUMMARY

Social play is pervasive in juvenile mammals, yet it is poorly understood in terms of its underlying brain mechanisms. Specifically, we do not know why young animals are most playful and why most adults cease to social play. Here, we analyze the synaptic mechanisms underlying social play. We found that blocking the rat periaqueductal gray (PAG) interfered with social play. Furthermore, an age-related decrease of neural firing in the PAG is associated with a decrease in synaptic release of glycine. Most importantly, modulation of glycine concentration—apparently acting on the glycinergic binding site of the N-methyl-D-aspartate (NMDA) receptor—not only strongly modulates social play but can also reverse the age-related decline in social play. In conclusion, we demonstrate that social play critically depends on the neurotransmitter glycine within the PAG.

INTRODUCTION

Social play is a repeated, incompletely functional behavior differing from more serious versions structurally, contextually, or ontogenetically, and is initiated voluntarily when the animal is in a relaxed or low-stress setting.[1] Social play behavior is widespread among young mammals and is also observed in other vertebrates and invertebrates,[1–3] but compared with other behaviors, it is still the least studied at the level of neural circuitry. Remarkably, we know very little about which brain areas are involved, and have no understanding of the molecular and cellular mechanisms underlying social play behavior.[1,4] On the one hand, the fact that vertebrates and invertebrates play suggests that this type of behavior is independent of brain type and has some common mechanisms at the molecular and cellular level. On the other hand, the social play has a structure that requires coordination and, consequently, certain play centers. Social play behavior is evolutionarily ancient among vertebrates and is found even in sharks,[1] therefore play initiating centers should also be phylogenetically ancient. In addition, social play, such as rough and tumble play, is related to inter-partner communication and the expression of emotions.[5] We hypothesized that the periaqueductal gray (PAG), a midbrain structure with a key role in the regulation of emotion and emotion-driven action selection,[6–8] as well as fight or flight behavior,[9,10] may also be crucial for the generation of social play behavior.[4]

Rough and tumble play (also called play fighting) is one of the most common forms of social play,[11] is particularly intense in juvenile mammals, and declines with age.[12,13] To identify the neural mechanisms involved, we used the age dependence of social play to identify candidate mechanisms that co-correlate with the age-related decline in playfulness. Our analysis shows that glycinergic (Gly) synaptic transmission is causally linked to the age-related decline of social play behavior.

RESULTS

Social play

First, we established an animal model for social play behavior (rough and tumble play) in rodents.[5,14] Figures 1A1 and 1A2 illustrates the three types of behavior (pouncing, pinning, and boxing) we considered as play behavior.[15–17] Play activity is defined as the summed time of pouncing, pinning, and boxing divided by the total time of observation.[16,18] Initially, we analyzed the behavior of mice—the most common animal model in neurosciences. However, mice showed a very limited amount of social play behavior (Figures 1B and 1C). In sharp contrast, play behavior was pronounced in male rats (Figures 1B and 1C, ANOVA F (2, 58) = 25.10, $p < 0.0001$). Non-playful social activity such as for example anogenital sniffing was comparable between male mice and rats (Figure 1D, Kruskal-Wallis statistic = 1.95, groups $n = 3$, $p = 0.4$). Therefore, we decided to continue our investigations on social

Please cite this article in press as: Dvorzhak et al., Social play behavior is driven by glycine-dependent mechanisms, Current Biology (2024), https://doi.org/10.1016/j.cub.2024.06.073

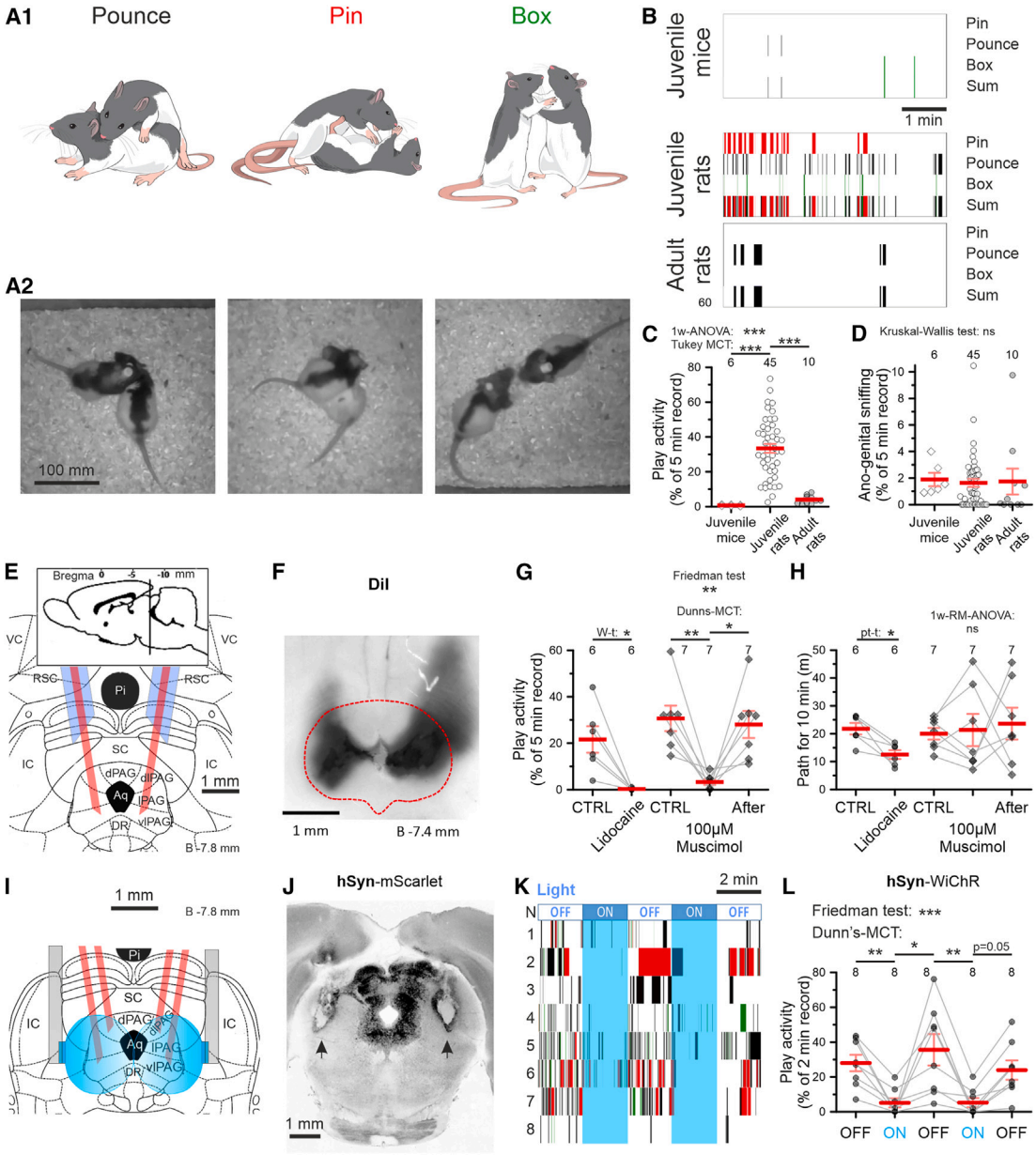

Figure 1. PAG is required for play behavior

(A) Rats play activity (A1, drawing; A2, photos) is defined as the accumulated time spent pouncing (left), pinning (middle), and boxing (right) divided by the total time of observation.

(B) Timeline histograms of different play activities and their sums for juvenile mice (top), juvenile (middle), and adult (bottom) rats.

(C) Juvenile (4–6 weeks) rats but not juvenile mice (5 weeks) show rough and tumble play, which is suppressed in adult rats (47–55 weeks).

(D) Juvenile mice and rats as well as adult rats spend similar time for anogenital sniffing, corresponding to non-playful social interactions.

(E) Based on the Paxinos atlas scheme of the implantation of the guiding cannulas (in blue) and the positioning of the injecting cannulas (in red).

(F) PAG photo showing the distribution of the green dye (DiI) injected bilaterally according to the scheme in (D). The red dotted line indicates the boundaries of the PAG.

(G) Bilateral injection of 2 μL of 2% lidocaine and 100 μM muscimol through guide cannulas into the PAG almost completely blocks play behavior in injected rat. The day after the muscimol injection, the rat's playfulness completely recovers, showing specificity of the effect to the drug but not to the PAG damage. CTRL means injection of isotonic 0.9% NaCl.

(H) In contrast to muscimol, lidocaine injection causes motor impairment, leading to a significant decrease in the distance traveled in the open field test.

(I) Scheme of LEDs implantation (the blue color indicates the approximate area of light irradiation) and AAV-hSyn-WiChR-mScarlet virus injection sites (injection cannulas are marked in red).

(J) Two-photon-image of PAG shows mScarlet expression 2 weeks after virus (AAV-hSyn-WiChR-mScarlet) injection. The arrows show the footprints of the implanted LEDs.

(legend continued on next page)

Please cite this article in press as: Dvorzhak et al., Social play behavior is driven by glycine-dependent mechanisms, Current Biology (2024), https://doi.org/10.1016/j.cub.2024.06.073

play behavior in male rats. Consistent with previous work,[13,19] we found a striking age-dependency of play (Figures 1B and 1C) with age-independent non-playful social activity (Figure 1D). Aggressive attacks, another non-playful social activity that may look like rough and tumble play but is distinguished from it by aggressive posturing, piloerection, serious biting, and so on,[20,21] are not observed in juvenile male rats,[13] but we also did not see them in our experiments with adults (Video S6). In the next set of experiments, we directly tested if the PAG is involved in social play. We used different pharmacological and optogenetic tools to analyze the role of the PAG in this type of behavior. Bilateral injection of the sodium channel blocker lidocaine through guide cannulas into the PAG almost completely blocks play behavior (Figures 1E–1G; Video S1, sum of signed ranks (W) = −21, $p = 0.03$). Lidocaine not only blocks spiking in the somatic and dendritic compartments but also the axonal propagation and could thus block play within the PAG in an unspecific manner. Indeed, lidocaine injection causes motor impairment, leading to a significant decrease in the distance traveled in the open field test (Figure 1H, Student's t test, t = 4, df = 5, $p = 0.01$). Therefore, we repeated the same type of experiment with the specific γ-aminobutyric acid (GABA)-a-receptor agonist muscimol. Muscimol (100 μM) also efficiently blocks social play (Figures 1E–1G; Video S2, Friedman statistic = 11, groups $n = 3$, $p = 0.0012$), but does not cause motor impairment (Figure 1H, ANOVA (1.168, 7.006) = 0.13, $p = 0.76$). It is important to point out that these experiments were completely reversible (Figure 1G). To further increase specificity, we performed optogenetic experiments with the recently developed potassium-based inhibitory opsin called WiChR[22] (see also Figure S1). Following an AAV-hSyn-WiChR-mScarlet virus injection, we implanted wireless light-emitting diodes (LEDs). Remarkably, light stimulation of WiChR expressed in PAG almost completely abolished play activity—in a reversible manner (Figures 1I–1L; Video S3, Friedman statistic = 25.2, groups $n = 5$, $p < 0.0001$).

Role of glycine in social play

In the next set of experiments, we investigated the molecular, cellular, and circuit mechanisms of social play. Since older rats are much less playful than younger ones, we recorded physiological activity from principal neurons within the PAG of juvenile and adult animals (see STAR Methods) and analyzed up to 178 different parameters of intrinsic and synaptic properties (Table S1) as well as their correlation with the playfulness of juvenile male rats. Although most parameters were not significantly different, we found a striking difference in firing properties of neurons of juvenile (playful) and adult animals (non-playful). Neurons from younger animals showed a spontaneous firing rate of up to 10 Hz (average: 1.39 ± 0.33 Hz, $n = 46$ neurons from 10 rats), whereas neurons from adult animals were almost silent (0.40 ± 0.18 Hz, $n = 26$ neurons from 6 rats) (Figures 2B and 2C; Table S1, t = 2.136, F (1, 70) = 4.6, $p = 0.036$). This spontaneous firing can be completely blocked by glutamatergic ionotropic receptor antagonists (L-(+)-2-Amino-5-phosphonopentanoic acid [APV] with 6,7-dinitroquinoxaline-2,3-dione [DNQX]) indicating the extrinsic nature of this firing as a projection of neural network activity in PAG (Figures S2A–S2C). Assessment of the tetrodotoxin (TTX)-sensitive fraction of spontaneous postsynaptic currents (sPSCs) in PAG slices shows a 39% suppression of excitatory neuronal activity in PAG networks (Figures S2D–S2F; Table S1), which cannot be explained by the inversion of GABA action (Figures S5A–S5C). Next, we wondered how these differences come about and if they are causally linked to social play behavior. In our detailed analysis of the physiological parameters (see above), which show significant age dependence and correlate with the playfulness of juvenile male rats in the same direction, the most significant difference between playful and non-playful male rats was found in Gly transmission (Table S1; Figure 2D). The frequency of Gly miniature inhibitory postsynaptic currents (Gly-mIPSCs) has a positive correlation with the playfulness of juvenile male rats (Table S1) and an age-related decrease from 1.16 ± 0.16 Hz to almost a complete loss of transmission (Figure 2E, nested t = 3.103, F (1, 32) = 9.6, $p = 0.004$). The very few remaining Gly-mIPSCs had a similar quantal amplitude (17.5 ± 1.9 pA, $n = 21$, Figure 2F; Table S1, nested t = 0.197, F (1, 31) = 0.039, $p = 0.85$). Moreover, Gly-IPSCs evoked by minimal electrical stimulation (Gly-eIPSCs) (Figures 2G–2I) show a 61% age-related decrease of amplitude (Figure 2J, Mann-Whitney U = 28, $p = 0.0015$) and a 68% age-related increase in the coefficient of variation (Figure 2L, t = 2.139, df = 25, $p = 0.042$) at age-independent paired pulse ratio (PPR; Figure 2K, Mann-Whitney U = 72, $p = 0.38$). All of this points to a reduced readily releasable pool (RRP) size of Gly inputs in adult male rats. Indeed, assessment of RRP based on the depletion of Gly inputs[23] with a 40 Hz minimal stimulation (Figures 3A and 3B), followed by plotting of a cumulative Gly-eIPSCs amplitude curve (see STAR Methods; Figures 3C and 3D), shows a 63% age-related decrease in RRP (Figure 3F), an age-independent quantal response size (Figure 3E) and age-independent release probability (Figure 3G).

Another reason for the decrease in Gly transmission could be the loss of Gly neurons. Indeed, immunohistochemical staining of PAG slices with antibodies against glycine and NeuN followed by confocal imaging (Figures S3A–S3F) reveals a 31% reduction of glycine-rich neurons in adult male rats (Figures S3B, S3C, and S3G).

We were puzzled by this strong decrease in Gly transmission, and wondered whether it might be related to the observed decrease in spontaneous spiking (Figures 2B, 2C, and S2D–S2F). Indeed, somewhat surprisingly, raising the level of extracellular glycine via the application of the glycine transporter 1 (GlyT1) inhibitor ALX-5407 triggered an increase in excitatory inputs on PAG neurons (Figures S2G and S2H). Furthermore, this effect of ALX-5407 was inhibited by blocking action potential firing with TTX and also by the application of the N-methyl-D-aspartate (NMDA) receptor antagonist MK-801 (Figure S2I). To understand the mechanisms of glycine action, we tested how the glycine receptors antagonist strychnine and the blocker of

(K) Scheme of optical stimulation with 468 nm light (top) and timeline histograms of play activity of the rats participated in the experiments. Color code: pouncing, black; pins, red; boxing, green.
(L) Optical suppression of PAG hSyn cells with of WiChR strongly reduces play activity in rats.
The gray lines on (G), (H), and (L) indicate paired measurements. ns, $p \geq 0.05$; *$p < 0.05$; **$p < 0.01$; ***$p < 0.001$.
See also Figure S1, Videos S1, S2, and S3, and Data S1.

Please cite this article in press as: Dvorzhak et al., Social play behavior is driven by glycine-dependent mechanisms, Current Biology (2024), https://doi.org/10.1016/j.cub.2024.06.073

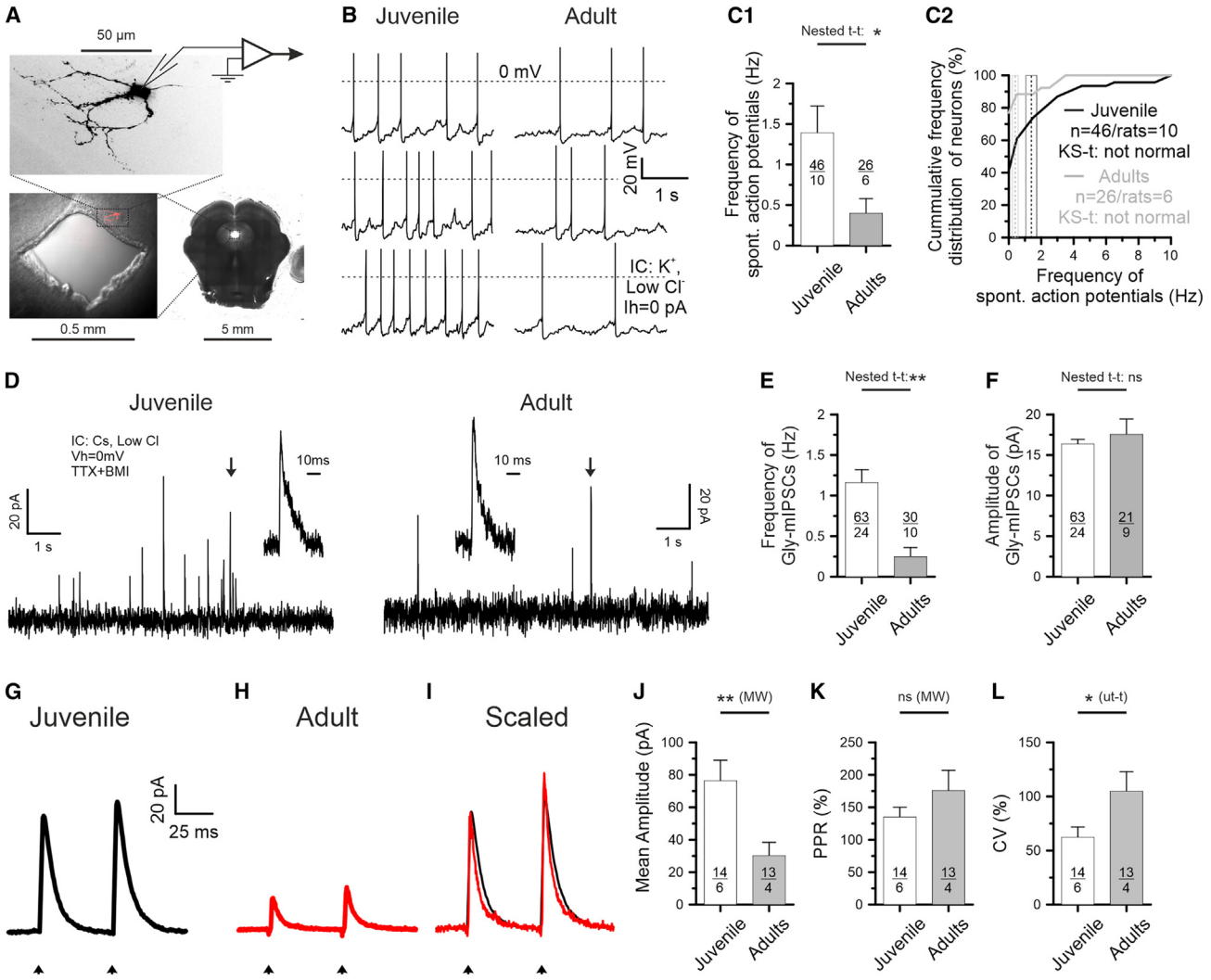

Figure 2. Age-related decrease of neural firing and synaptic Gly release in the PAG

(A) Midbrain coronal slice image showing the location of the recorded cell filled with Alexa-594.

(B) Traces of membrane potentials recorded in CC-mode ($I_{holding}$ = 0 pA) in dlPAG neurons from juvenile (top) and adult rats (bottom).

(C1 and C2) The spontaneous neuronal firing frequency statistics show a significant age-dependent decrease of neuronal activity in PAG. (C1) shows the comparison of mean values; (C2) shows the cumulative distribution.

(D) Traces of glycinergic inhibitory postsynaptic membrane currents recorded at 0 mV holding potential in the presence of 1 μM TTX and 20 μM bicuculline (BMI) in PAG neurons from juvenile (left) and adult (right) rat slices. The insets show an enlarged Gly-IPSC marked with an arrow.

(E) The frequency of miniature Gly-IPSCs demonstrate a significant age-dependent decrease.

(F) The amplitude of miniature Gly-IPSCs show that the quantal size of synaptic glycine release is independent of age.

(G–I) Examples of glycinergic IPSCs (Gly-IPSCs) evoked by minimal paired at 20 Hz electrical stimulation and recorded with low Cl intracellular pipette solution at 0 mV in the presence of 20 μM BMI in caudal-dlPAG neurons of juvenile (G) and adult (H) rats. The gray thin traces show responses to individual stimuli (60 entries). The thicker traces (black for juvenile, red for adult) represent the average traces. (I) shows the same averaged traces, but scaled by the first response. The arrows indicate the removed stimulation artifacts.

(J) The averaged Gly-eIPSCs amplitudes show a significant age-related decrease.

(K) The paired pulse ratio (PPR) of Gly-eIPSCs does not change significantly with age.

(L) The coefficient of variation (CV) of Gly-eIPSCs significantly increases with age, indicating, together with the PPR (E), a reduction in the readily releasable pool (RRP) of glycinergic synaptic vesicles with age.

ns, $p \geq 0.05$; *$p < 0.05$; **$p < 0.01$. See also Figures S2 and S5 and Table S1 and Data S1.

the glycine-binding site on NMDA receptors HA-966 influence neuronal activity in PAG slices. Strychnine does not alter the frequency of spontaneous excitatory postsynaptic currents (sEPSCs) (Figures S2K–S2M), although it does reduce the frequency of spontaneous IPSCs (sIPSCs) (Figures S2K, S2L, and S2N). By contrast, HA966 reduces the frequency of both sEPSCs and sIPSCs (Figures S2O–S2T). The suppression of sEPSCs by HA966 decreases with age, whereas the suppression of sIPSCs is age independent (Figures S2O–S2R and S2U). Therefore, HA966 reduces the ratio between excitation and inhibition (E/I)

Please cite this article in press as: Dvorzhak et al., Social play behavior is driven by glycine-dependent mechanisms, Current Biology (2024), https://doi.org/10.1016/j.cub.2024.06.073

CellPress
OPEN ACCESS

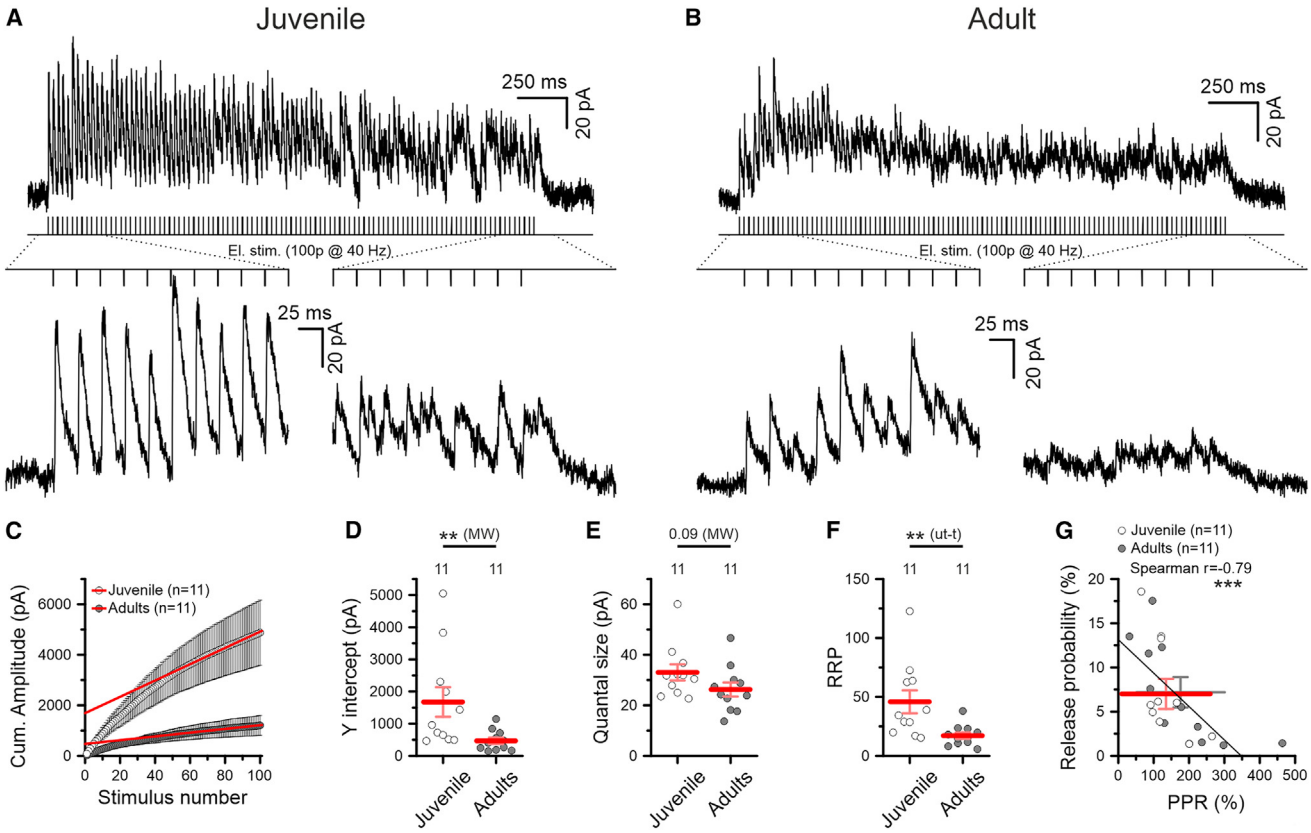

Figure 3. Assessment of the readily releasable pool size for glycinergic inputs in the PAG

(A and B) Examples of Gly-IPSCs induced with high-frequency (40 Hz) electrical stimulation (100 pulses) of caudal-dlPAG neurons from juvenile (A) and adult (B) rats. The upper traces show stimulation entirely. The bottom left traces show the first 10 stimuli, the bottom right traces show the last 10 stimuli.

(C) The plot of cumulative amplitudes shows a linear increase after 50 pulses, indicating depletion of the readily releasable pool (RRP) for both the juvenile (white circles) and adult (gray circles) rat groups. The red lines represent these linear trends.

(D) Y intercepts of the linear components in the cumulative amplitude curves indicate a significant decrease in the product of quantal size and RRP in adult rats. t = 2.6, df = 20, $p = 0.02$, Cohen's d = 1.

(E) The quantal response size, defined as the average amplitude of synchronous Gly-IPSCs over the last 50 pulses, shows no age dependence. Mann-Whitney U = 34, $p = 0.09$, Cohen's d = 0.68.

(F) The readily releasable pool (RRP) size, calculated as the ratio of Y-intercept to quantal size, is significantly reduced in adult rats t = 2.8, df = 20, $p = 0.01$, Cohen's d = 1.2.

(G) The release probability (Pr) calculated as the ratio of the average amplitude 1 to the Y-intercept is negatively correlated with PPR, showing a good relationship between the two different methods of estimating real Pr. The horizontal lines showing the mean ± SE for Pr show no age-related changes, as well as the mean PPR values shown by the vertical lines. For release probability Mann-Whitney U = 58, $p = 0.9$.

$^{**}p < 0.01$; $^{***}p < 0.001$.See also Figure S3 and Data S1.

in PAG slices only from juvenile, but not from adult male rats (Figures S2O–S2R and S2V). Taken together, an age-dependent decrease in firing rate correlates with a collapse of Gly activity—most likely via the glycine-binding site of NMDA receptors.

To test a causal relationship of glycine and social play behavior, we established *in vivo* experiments with pharmacological manipulations and behavioral readouts. Indeed, blocking of astrocytic glycine transporters (GlyT1), with ALX-5407 strongly enhanced social play (Figures 4A1 and 4A3; Video S4, F (2.311, 16.18) = 7.44, $p = 0.004$). However, GlyT1 can operate both in the uptake mode and release glycine from astrocytes.[24] To resolve this uncertainty, we applied the neurotransmitter itself, which resulted in an up to 3-fold overall increase of social play (Figures 4A1 and 4A3; Video S4). The unidirectional effects of the GlyT1 blocker itself and together with glycine demonstrate the uptake mode of transporters in rest. In both cases, general motor activity (Figures 4A2 and 4A4, Friedman statistic = 1.86, $p = 0.6$) and percent of time in the central area (Figure S4G) in the open field test were not altered, nor was anogenital sniffing (Figures S4A and S4B), an example of non-playful social activity. Consistent with the NMDA-dependent mechanism suggested by our *in vitro* data, this effect could be blocked by the NMDA receptor antagonist MK-801 and also by the blocker of the glycine-binding site on the NMDA receptor HA-966, but not by the glycine receptor antagonist strychnine (Figures 4B1–4B4, S4C, S4D, and S4H; Video S5; for Figure 4B3: F (2.203, 17.62) = 5.89, $p = 0.0095$, for Figure 4B4: F (1.903, 15.22) = 1.49, $p = 0.26$).

If indeed the age-dependent reduction in glycine signaling we observed *in vitro* is responsible for the reduction of playfulness in

Please cite this article in press as: Dvorzhak et al., Social play behavior is driven by glycine-dependent mechanisms, Current Biology (2024), https://doi.org/10.1016/j.cub.2024.06.073

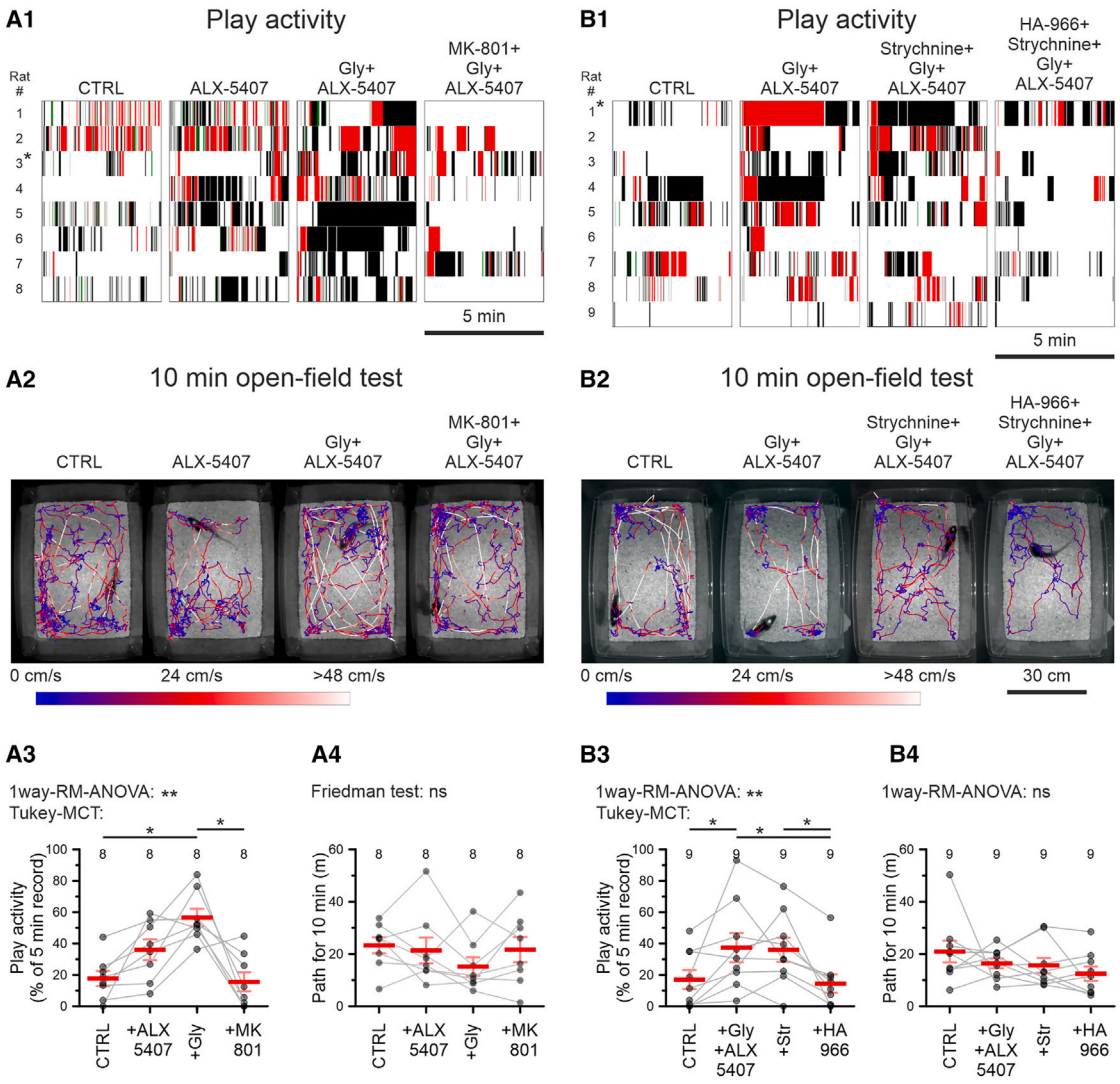

Figure 4. Increasing glycinergic transmission boosts play via the glycinergic site of the NMDA receptor

(A) Glycine stimulates rough and tumble play in juvenile rats. Rats were injected into PAG via guide cannulas with 0.9% NaCl control solution (CTRL), 2 μM ALX-5407, a mixture of ALX-5407with 100 μM glycine, and a mixture of the previous solution with an NMDA receptor blocker, 10 μM MK-801.

(A1) Timeline histograms of play activity for different rats after injections.

(A2) Pathways traveled by the rat indicated with the asterisk in (A1) in a 10-min open-field test after injections.

(A3) The statistics for the data in (A1) show a significant and unidirectional increase in play activity of juvenile rats following injections of the inhibitor GlyT1 (ALX-5407) and its mixture with glycine (Gly). This effect can be completely blocked by the NMDA receptor blocker (MK-801).

(A4) The statistics of the 10 min traveled path in the open field test show no significant effect of injecting all the above substances into the PAG on the rats' motor activity.

(B) Glycine stimulates play via NMDA receptors. Rats were injected into PAG via guide cannulas with control solution (CTRL), a mixture of 2 μM ALX-5407 with 100 μM glycine, a mixture of the previous substances with 2 μM strychnine (Str), Gly-receptor blocker and a mixture of all of the above with 400 μM HA-966, a blocker of Gly-binding site on NMDA receptor.

(B1) Timeline histograms of play activity after injections.

(B2) Pathways traveled by the rat indicated with the asterisk in (B1) in a 10-min open-field test after injections.

(B3) The statistics for the data in (B1) show that the glycine-induced increase of play activity can be blocked by blocking of NMDA receptors, but not by blocking glycine receptors.

(B4) The statistics of the traveled path in the open field test show no significant effect of injecting the substances mentioned above into the PAG on the motor activity of juvenile rats.

The gray lines on (A3), (A4), (B3), and (B4) indicate paired measurements.

Color code: pouncing, black; pins, red; boxing, green.

ns, $p \geq 0.05$; *$p < 0.05$; **$p < 0.01$. See also Figure S4, Videos S4 and S5 and Data S1.

Please cite this article in press as: Dvorzhak et al., Social play behavior is driven by glycine-dependent mechanisms, Current Biology (2024), https://doi.org/10.1016/j.cub.2024.06.073

CellPress
OPEN ACCESS

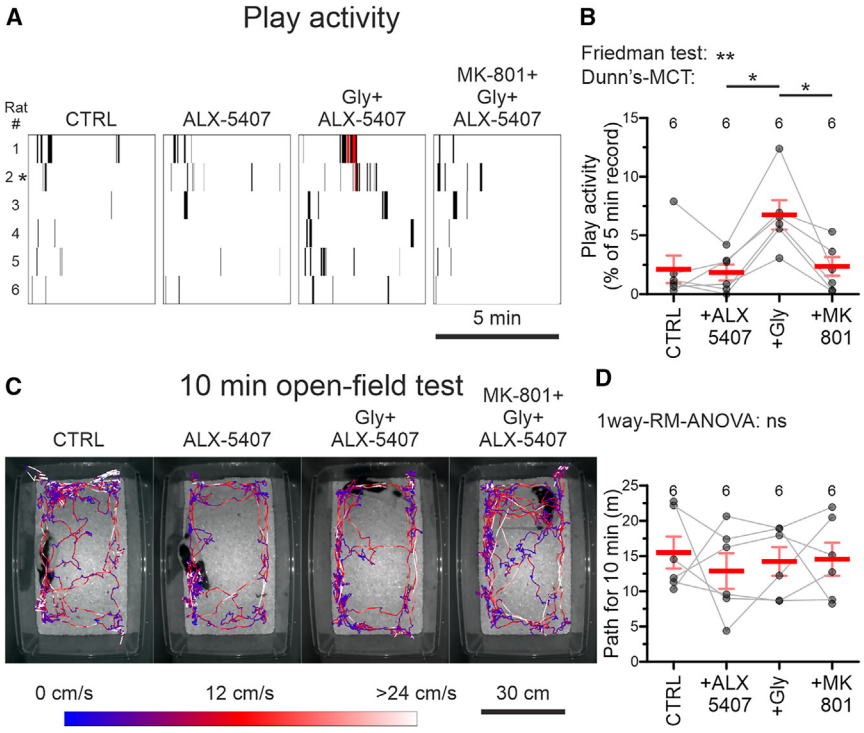

Figure 5. Glycine stimulation of play activity in adult rats

(A) Timeline histograms of play activity for adult rats immediately after injections in PAG via guide cannulas of 0.9% NaCl control solution (CTRL), 2 μM ALX-5407, GlyT1 blocker, a mixture of the previous substance with 100 μM glycine (Gly), and a mixture of all of the substances mentioned above with an NMDA receptor blocker, 10 μM MK-801. Asterisk points to the rat whose data are shown in (B). Color code: pouncing, black; pins, red; boxing, green.

(B) The statistics for the data in (A) show a significant increase in play activity of adult rats following injections of the inhibitor GlyT1 (ALX-5407) mixed with glycine (Gly) but not after injection of ALX-5407 alone. This effect of Gly can be completely blocked by the NMDA receptor blocker (MK-801). Friedman statistic = 11, $p = 0.006$.

(C) Pathways of the adult rat labeled in (A) by asterisk in 10-min open-field tests, 10 min after injections of 0.9% NaCl solution (CTRL), 2 μM ALX-5407, a mixture of the previous substance with 100 μM glycine (Gly), and a mixture of all of the above with 10 μM MK-801.

(D) The statistics of the 10 min path in the open field test show no significant effect of injecting all the above substances into the PAG on the motor activity of adult rats. F (1.210, 6.052) = 0.28, $p = 0.7$. The gray lines on (B) and (D) indicate paired measurements.

ns, $p \geq 0.05$; *$p < 0.05$; **$p < 0.01$. See also Figure S4 and Video S6 and Data S1.

older animals, we wondered whether it might be possible to make older rats playful again by manipulating glycine concentration in the PAG. Strikingly, this was indeed the case: locally applied ALX-5407, when combined with glycine, made non-players play again—an effect which was NMDA receptor dependent (Figures 5, S4E, S4F, and S4I; Video S6).

DISCUSSION

PAG is necessary for play

The present study investigated the mechanisms of age-related decline in social play behavior, in which we focused on the PAG. A variety of observations point to non-forebrain structures as driver of social play behavior, e.g., decorticated rats[25] or rats with damaged amygdala[26] or basal ganglia[27,28] remain playful, which does not exclude modulatory function of the forebrain on social play.[29,30] The involvement of different midbrain structures in playful behavior has previously been shown by c-*fos* gene expression.[31] Among these structures, PAG attracts special attention because it is the output, decision-making structure of neural networks determining many social behaviors.[32] Moreover, neural activity is increased in the PAG during laughter or tickling in humans[33] and hand chasing play in rats.[4] This study presents evidence for the necessity of PAG for social play behavior. Thus, specific suppression of PAG neuron activity by lidocaine, muscimol, or optogenetic methods almost completely blocks rough and tumble play. Nevertheless, as previously shown, PAG is involved in the formation of instinctive responses that themselves may influence social play behavior, such as anxiety,[34] fear,[35] social fear,[32,36] etc. These collateral reactions are antagonistic to social play behavior, and hence when PAG is silenced they should also be suppressed, which in turn should reinforce social play behavior, but we observe the opposite. Moreover, most of these collateral reactions cause disturbance of general motor activity (e.g., freezing or anxiety) or non-playful social activity (social fear), but we do not observe a significant change between different phases of illumination or after muscimol injections in the open field tests (Figures 1E–1L and S1G–S1J). Since the PAG is critically involved in the initiation of social play behavior, age-related changes in PAG are possibly associated with age-related declines in playfulness.

Intrinsic PAG factors leading to social play decline with age

Next, to identify the characteristics of PAG networks related to social play, we determined the electrophysiological correlates of social play and examined the age dependence of these correlates using the patch-clamp method. Despite many parameters correlating with social play and being age-dependent, only one parameter (Gly-mIPSCs frequency), characterizing Gly synaptic transmission, is significantly positively correlated with social play and decreases with age (Table S1). Of course, we do not claim that this is the only parameter related to social play behavior, but it is an important physiological response characteristic that impacts on the operation of PAG networks. In line with this idea, we demonstrate that the inhibitory mediator glycine shifts the balance of E/I in PAG networks toward excitation using NMDA receptors via the glycine-binding domain (Figures S2G–S2V), thereby increasing general neuronal activity of PAG

Please cite this article in press as: Dvorzhak et al., Social play behavior is driven by glycine-dependent mechanisms, Current Biology (2024), https://doi.org/10.1016/j.cub.2024.06.073

networks (Figures 2A–2C and S2D–S2F) and stimulating rats to engage in social play (Figures 4 and 5).

Our data also show a strong age-related decline in Gly synaptic transmission (Figures 2D–2F), leading to decreased NMDA receptor activation via Gly-binding domain (Figures S2U and S2V), reduced neuronal activity (Figures S2S and S2T) in the PAG and resulting in decreased social play activity (Figure 1C). Moreover, there are no significant age-related changes in basal membrane properties (Table S1) or amplitude of Gly-mIPSCs (Figure 2F), which is mainly determined by postsynaptic receptors. An age-related decline in NMDA receptor expression could also explain the decrease in their activation, but such a mechanism is inconsistent with radio-ligand labeling data.[37] In addition to decreased NMDA receptors activation with age, neuronal activity may decrease due to age-related changes in firing properties, properties of synaptic inputs, inversion of chlorine currents, and strength of tonic GABA currents. Indeed, among other unchanged firing properties, rheobase significantly increases with age, which, on the background of unchanged basic membrane properties, can also be a result of decreased activation of NMDA receptors (Table S1). Analysis of miniature currents in the presence of TTX also indicates the absence of age-related changes in the properties of synaptic inputs (Table S1). Likewise, the strength of tonic GABAergic currents in PAG slices is age independent (Table S1; Figures S5D and S5E). Although the exact age of chloride current inversion in the PAG remains understudied, it is to be expected within the first 3 weeks of postnatal development as in other parts of the brain.[38] Indeed, bicuculline applied to PAG slices from male rats at 4 weeks of age induces an increase in sEPSCs (Figures S5A–S5C), indicating the inhibitory nature of GABA already in the juvenile period. Thus, we can conclude that one of the key intrinsic PAG factors determining the age-dependent decrease in neuronal PAG network activity is reduced NMDA receptor activation by glycine.

The most likely reason for the age-related decline in Gly neurotransmission is a reduction in the total RRP (Figure 3). Gly neurons create varicose terminals on which synapses occur predominantly[39] and likely have multiple contacts with postsynaptic cells, which are sensed by this cells as one large synapse. The age-dependent RRP reduction cannot be attributed to intrasynaptic maturation or synaptic pruning. This scenario seems unlikely, since a strong depletion of RRP at each individual synapse would have to lead to a change in PPR,[40] which we do not observe. In addition, we observe a 30% reduction in the number of glycine neurons in PAG slices with age (Figure S3), whereas the density of NeuN+ neurons remained unchanged (Figure S3H). It is also possible that "dilution" of glycine neurons and synaptic pruning together are responsible for the decrease in the number of Gly synapses per postsynaptic cell in the PAG with age.

Role of glycine and NMDA receptors in social play

PAG injection experiments *in vivo* confirmed a causal link between glycine-induced NMDA-receptors potentiation and social play behavior. However, glycine and GlyT1 blocker can stimulate social play through attenuation of antagonistic responses, such as anxiety and social fear. However, after the respective injections we do not see significant change in the time of anogenital sniffing, which inversely characterizes social fear (Figures S4A–S4D), as well as in the percentage of time animals spend in the central area in the open-field test which characterizes anxiolytic effects (Figures S4G and S4H). If anything, Gly and ALX-5407 show an anxiogenic effects.

It should also be noted that injected NMDA receptor blockers did not completely suppress the social play behavior in all cases. On the one hand, this may reflect imperfect injections in which the blockers did not reach all receptors. On the other hand, it may point to NMDA-independent mechanisms of social play behavior. However, experiments with intraperitoneal administration of the NMDA receptor blocker MK801 completely and specifically suppresses social play activity in rats,[41] contradicting such a hypothesis.

Most surprisingly, we were able to recover playful behavior in adult animals via pharmacological manipulation of the PAG glycine level (Figures 5, S4E, S4F, and S4I; Video S6). On the one hand, this suggests the functionality of social play networks in the PAG of adult rats and the modulating role of glycine in it. On the other hand, the failure of glycine to fully restore playfulness suggests other age-dependent factors acting on social play behavior.

However, the age at which rats become fully adult is not certain; many researchers believe that adulthood begins at 2–3 months of age.[42,43] Nevertheless, although rats appear physiologically and behaviorally to be adults after the third months of life, they continue to develop socially and form hierarchies, which is reflected in changes in play content.[44] Adult social play differs from adolescent play not only in form but also in essence and offers adults far fewer benefits than adolescents.[45] The choice of the adult age for rats in our work (6 months), is due to the publication of Sengupta[46] who related 6-month-old rats with 18 years of human life.

Other age-related factors that reduce social play may include the hormonal rise during the peri-puberty. Indeed, the sex component of playfulness reverses with age after the onset of sexual differentiation.[13,19] Nevertheless, the fact that play behavior in rats is sex-independent in early adolescence,[19] when sex hormones are at the same low level in both sexes, indicates a principal similarity in the structure of neuronal play networks between the sexes.[13] Testosterone, which is absent in females and at about 30% of its maximum in male rats throughout adolescence,[13] apparently stimulates playfulness.[47,48] The age-dependent sex-specific suppression of playfulness in rats is possibly associated with increased levels of female hormones during adolescence. This is supported by the suppressive effect of estradiol[49,50] and progesterone on NMDA receptors.[51] Nevertheless, the age dependence of the sex difference of playfulness requires further studies.

Opioids and cannabinoids have been shown to stimulate social play behavior via the reward system.[52,53] Dopamine stimulates the motivation for social play.[53,54] Noradrenaline, serotonin, and vasopressin systems have a complex and not yet fully explored pharmacology of modulation of social play.[53] However, the social play pharmacology of these neurotransmitters has been studied at a systemic level or in relation to forebrain structures (modulatory structures in relation to social play), making it difficult to understand their mechanisms of action on the initiation of social play. In all of this glycine is a novel and probably very significant pharmacological determinant of social play behavior.

Social play activity peaks in the juvenile to prepubertal period[13] roughly coinciding with the peak of neural network

shaping and synaptic pruning[55] guided by synaptic activity.[56] Glycine has the unique ability to support active synapses via NMDA receptors and in parallel increase neuronal threshold via glycine receptors, thereby cutting off weak inputs, which generally facilitates synaptic selection. Consistent with our findings, glycine increases neuronal activity, at least in PAG networks, and stimulates social play behavior. Glycine has also been shown to act as an attractant[57] and activator of microglia,[58] the main "gardener" in brain tissue.[59] Taken together, our data suggest that glycine coordinates playful behavior.

Conclusions

The critical role of the PAG in rat social play is consistent with previous work showing that the PAG is a critical gating structure for a range of emotion-driven behaviors.[6,7,32] Glycine-mediated modulation of NMDA receptors has previously been linked to social behavior[60] and is widely distributed in all parts of the mammalian brain and invertebrate ganglia.[61,62] A partial agonist of the Gly NMDA site has been proposed as an aid in the treatment of depression, autism, and post-traumatic stress disorder.[63–65] Our findings on the mechanisms of social play in rodents may therefore have implications for understanding conditions, such as depression and autism, in which social play is degraded.[64,66–69] Finally, although play has long been neglected as a topic of serious scientific study, we believe a deeper understanding of playfulness may be a key to understanding human nature and culture (too crazy to cite e.g. Huizinga, "Homo ludens"[70]). Our study is not only one of the first analyses of the synaptic mechanisms of social play, but will also hopefully trigger further investigations on the functional role of social play and of the PAG.

STAR★METHODS

Detailed methods are provided in the online version of this paper and include the following:

- KEY RESOURCES TABLE
- RESOURCE AVAILABILITY
  - Lead contact
  - Materials availability
  - Data and code availability
- EXPERIMENTAL MODEL AND STUDY PARTICIPANT DETAILS
- METHOD DETAILS
  - Surgery
  - Implantation of guide cannulas and deep brain injections
  - Optogenetics
  - Behavior
  - Electrophysiology
  - Pharmacology
  - Immunohistochemistry
  - Confocal microscopy
- QUANTIFICATION AND STATISTICAL ANALYSIS

SUPPLEMENTAL INFORMATION

Supplemental information can be found online at https://doi.org/10.1016/j.cub.2024.06.073.

ACKNOWLEDGMENTS

The authors thank Susanne Rieckmann and Anke Schönherr for excellent technical assistance. We are indebted to John Tukker for helpful comments on the manuscript and to Antje Fortströer for assistance with manuscript preparation. This study was supported by the German Research Foundation (Deutsche Forschungsgemeinschaft [DFG], project 184695641—SFB 958, project 327654276—SFB 1315, project 415914819—FOR 3004, project 431572356, and Germany's Excellence Strategy—Exc-2049-390688087), by the Federal Ministry of Education and Research (BMBF, SmartAge—project 01GQ1420B), and by the European Research Council (ERC) under the European Union's Horizon 2020 research and innovation program (grant agreement no. 810580).

AUTHOR CONTRIBUTIONS

Conceptualization: D.S., M.B., and A.D.; methodology: A.D.; software: A.D.; validation: A.D.; formal analysis: A.D.; investigation: A.D.; resources: A.D. and D.S.; data curation: A.D.; writing – original draft: D.S. and A.D.; writing – review & editing: D.S., A.D., and M.B.; visualization: A.D. and D.S.; supervision: D.S.; project administration: D.S.; funding acquisition: D.S. and M.B.; supervision: D.S.

DECLARATION OF INTERESTS

The authors declare no competing interests.

Received: May 17, 2024
Revised: June 19, 2024
Accepted: June 27, 2024
Published: July 24, 2024

REFERENCES

1. Burghardt, G.M. (2005). The Genesis of Animal Play: Testing the Limits (The MIT Press).
2. Hanlon, R.T. (1996). Evolutionary Games That Squids Play: Fighting, Courting, Sneaking, and Mating Behaviors Used for Sexual Selection in Loligo pealei. Biol. Bull. *191*, 309–310. https://doi.org/10.1086/BBLv191n2p309.
3. Galpayage Dona, H.S., Solvi, C., Kowalewska, A., Mäkelä, K., MaBouDi, H., and Chittka, L. (2022). Do bumble bees play? Anim. Behav. *194*, 239–251. https://doi.org/10.1016/j.anbehav.2022.08.013.
4. Gloveli, N., Simonnet, J., Tang, W., Concha-Miranda, M., Maier, E., Dvorzhak, A., Schmitz, D., and Brecht, M. (2023). Play and tickling responses map to the lateral columns of the rat periaqueductal gray. Neuron *111*, 3041–3052.e7. https://doi.org/10.1016/j.neuron.2023.06.018.
5. Palagi, E., Burghardt, G.M., Smuts, B., Cordoni, G., Dall'Olio, S., Fouts, H.N., Řeháková-Petrů, M., Siviy, S.M., and Pellis, S.M. (2016). Rough-and-tumble play as a window on animal communication. Biol. Rev. Camb. Philos. Soc. *91*, 311–327. https://doi.org/10.1111/brv.12172.
6. Venkatraman, A., Edlow, B.L., and Immordino-Yang, M.H. (2017). The Brainstem in Emotion: A Review. Front. Neuroanat. *11*, 15. https://doi.org/10.3389/fnana.2017.00015.
7. Zelena, D., Menant, O., Andersson, F., and Chaillou, E. (2018). Periaqueductal gray and emotions: the complexity of the problem and the light at the end of the tunnel, the magnetic resonance imaging. Endocr. Regul. *52*, 222–238. https://doi.org/10.2478/enr-2018-0027.
8. Burgdorf, J.S., and Moskal, J.R. (2023). A prefrontal cortex alpha/delta switch controls the transition from positive to negative affective states. Discov. Ment. Health *3*, 19. https://doi.org/10.1007/s44192-023-00044-3.
9. Evans, D.A., Stempel, A.V., Vale, R., and Branco, T. (2019). Cognitive Control of Escape Behaviour. Trends Cogn. Sci. *23*, 334–348. https://doi.org/10.1016/j.tics.2019.01.012.
10. Evans, D.A., Stempel, A.V., Vale, R., Ruehle, S., Lefler, Y., and Branco, T. (2018). A synaptic threshold mechanism for computing escape decisions. Nature *558*, 590–594. https://doi.org/10.1038/s41586-018-0244-6.
11. Aldis, O. (1975). Play Fighting (Academic Press Inc).
12. Pellis, S.M., and Pellis, V.C. (1998). Play fighting of rats in comparative perspective: a schema for neurobehavioral analyses. Neurosci. Biobehav. Rev. *23*, 87–101. https://doi.org/10.1016/s0149-7634(97)00071-7.

13. Bell, M.R. (2018). Comparing Postnatal Development of Gonadal Hormones and Associated Social Behaviors in Rats, Mice, and Humans. Endocrinology *159*, 2596–2613. https://doi.org/10.1210/en.2018-00220.

14. Pellis, S.M., Pellis, V.C., Ham, J.R., and Achterberg, E.J.M. (2022). The rough-and-tumble play of rats as a natural behavior suitable for studying the social brain. Front. Behav. Neurosci. *16*, 1033999. https://doi.org/10.3389/fnbeh.2022.1033999.

15. Panksepp, J., Siviy, S., and Normansell, L. (1984). The psychobiology of play: Theoretical and methodological perspectives. Neurosci. Biobehav. Rev. *8*, 465–492. https://doi.org/10.1016/0149-7634(84)90005-8.

16. Pellis, S.M., Pellis, V.C., Burke, C.J., Stark, R.A., Ham, J.R., Euston, D.R., and Achterberg, E.J.M. (2022). Measuring Play Fighting in Rats: A Multilayered Approach. Curr. Protoc. *2*, e337. https://doi.org/10.1002/cpz1.337.

17. Cooper, M.A., Grizzell, J.A., Whitten, C.J., and Burghardt, G.M. (2023). Comparing the ontogeny, neurobiology, and function of social play in hamsters and rats. Neurosci. Biobehav. Rev. *147*, 105102. https://doi.org/10.1016/j.neubiorev.2023.105102.

18. VanRyzin, J.W., Marquardt, A.E., and McCarthy, M.M. (2020). Assessing Rough-and-tumble Play Behavior in Juvenile Rats. Bio Protoc. *10*, e3481. https://doi.org/10.21769/BioProtoc.3481.

19. Loranca, A., Torrero, C., and Salas, M. (1999). Development of play behavior in neonatally undernourished rats. Physiol. Behav. *66*, 3–10. https://doi.org/10.1016/s0031-9384(98)00235-2.

20. Takahashi, A., and Miczek, K.A. (2014). Neurogenetics of aggressive behavior: studies in rodents. Curr. Top. Behav. Neurosci. *17*, 3–44. https://doi.org/10.1007/7854_2013_263.

21. Blanchard, R.J., and Blanchard, D.C. (1977). Aggressive behavior in the rat. Behav. Biol. *21*, 197–224. https://doi.org/10.1016/s0091-6773(77)90308-x.

22. Vierock, J., Shiewer, E., Grimm, C., Rozenberg, A., Chen, I.-W., Tillert, L., Castro Scalise, A.G., Casini, M., Augustin, S., Tanese, D., et al. (2022). WiChR, a highly potassium-selective channelrhodopsin for low-light one- and two-photon inhibition of excitable cells. Sci. Adv. *8*, eadd7729. https://doi.org/10.1126/sciadv.add7729.

23. Kaeser, P.S., and Regehr, W.G. (2017). The readily releasable pool of synaptic vesicles. Curr. Opin. Neurobiol. *43*, 63–70. https://doi.org/10.1016/j.conb.2016.12.012.

24. Reimer, A.E., Oliveira, A.R., and Brandao, M.L. (2008). Selective involvement of GABAergic mechanisms of the dorsal periaqueductal gray and inferior colliculus on the memory of the contextual fear as assessed by the fear potentiated startle test. Brain Res. Bull. *76*, 545–550.

25. Panksepp, J., Normansell, L., Cox, J.F., and Siviy, S.M. (1994). Effects of neonatal decortication on the social play of juvenile rats. Physiol. Behav. *56*, 429–443. https://doi.org/10.1016/0031-9384(94)90285-2.

26. Daenen, E.W.P.M., Wolterink, G., Gerrits, M.A.F.M., and Van Ree, J.M. (2002). The effects of neonatal lesions in the amygdala or ventral hippocampus on social behaviour later in life. Behav. Brain Res. *136*, 571–582. https://doi.org/10.1016/s0166-4328(02)00223-1.

27. Pellis, S.M., Castañeda, E., McKenna, M.M., Tran-Nguyen, L.T., and Whishaw, I.Q. (1993). The role of the striatum in organizing sequences of play fighting in neonatally dopamine-depleted rats. Neurosci. Lett. *158*, 13–15. https://doi.org/10.1016/0304-3940(93)90600-p.

28. Siviy, S.M. (2019). Basal ganglia involvement in the playfulness of juvenile rats. J. Neurosci. Res. *97*, 1521–1527. https://doi.org/10.1002/jnr.24475.

29. Siviy, S.M., and Panksepp, J. (2011). In search of the neurobiological substrates for social playfulness in mammalian brains. Neurosci. Biobehav. Rev. *35*, 1821–1830. https://doi.org/10.1016/j.neubiorev.2011.03.006.

30. Pellis, S., and Pellis, V. (2013). The Playful Brain: Venturing to the Limits of Neuroscience (Oneworld Publications).

31. Gordon, N.S., Kollack-Walker, S., Akil, H., and Panksepp, J. (2002). Expression of c-fos gene activation during rough and tumble play in juvenile rats. Brain Res. Bull. *57*, 651–659. https://doi.org/10.1016/s0361-9230(01)00762-6.

32. Chen, P., and Hong, W. (2018). Neural Circuit Mechanisms of Social Behavior. Neuron *98*, 16–30. https://doi.org/10.1016/j.neuron.2018.02.026.

33. Wattendorf, E., Westermann, B., Fiedler, K., Kaza, E., Lotze, M., and Celio, M.R. (2013). Exploration of the neural correlates of ticklish laughter by functional magnetic resonance imaging. Cereb. Cortex *23*, 1280–1289. https://doi.org/10.1093/cercor/bhs094.

34. Taylor, N.E., Pei, J., Zhang, J., Vlasov, K.Y., Davis, T., Taylor, E., Weng, F.-J., Van Dort, C.J., Solt, K., and Brown, E.N. (2019). The Role of Glutamatergic and Dopaminergic Neurons in the Periaqueductal Gray/Dorsal Raphe: Separating Analgesia and Anxiety. eNeuro *6*, ENEURO.0018-18.2019. https://doi.org/10.1523/ENEURO.0018-18.2019.

35. Vaaga, C.E., Brown, S.T., and Raman, I.M. (2020). Cerebellar modulation of synaptic input to freezing-related neurons in the periaqueductal gray. eLife *9*, e54302. https://doi.org/10.7554/eLife.54302.

36. Alfieri, V., Mattera, A., and Baldassarre, G. (2022). Neural Circuits Underlying Social Fear in Rodents: An Integrative Computational Model. Front. Syst. Neurosci. *16*, 841085. https://doi.org/10.3389/fnsys.2022.841085.

37. Kito, S., Miyoshi, R., and Nomoto, T. (1990). Influence of age on NMDA receptor complex in rat brain studied by in vitro autoradiography. J. Histochem. Cytochem. *38*, 1725–1731. https://doi.org/10.1177/38.12.2147708.

38. Dehorter, N., Vinay, L., Hammond, C., and Ben-Ari, Y. (2012). Timing of developmental sequences in different brain structures: physiological and pathological implications. Eur. J. Neurosci. *35*, 1846–1856. https://doi.org/10.1111/j.1460-9568.2012.08152.x.

39. Rampon, C., Luppi, P.H., Fort, P., Peyron, C., and Jouvet, M. (1996). Distribution of glycine-immunoreactive cell bodies and fibers in the rat brain. Neuroscience *75*, 737–755. https://doi.org/10.1016/0306-4522(96)00278-3.

40. Zucker, R.S., and Regehr, W.G. (2002). Short-term synaptic plasticity. Annu. Rev. Physiol. *64*, 355–405. https://doi.org/10.1146/annurev.physiol.64.092501.114547.

41. Siviy, S.M., Line, B.S., and Darcy, E.A. (1995). Effects of MK-801 on rough-and-tumble play in juvenile rats. Physiol. Behav. *57*, 843–847. https://doi.org/10.1016/0031-9384(94)00361-8.

42. Bishnoi, I.R., Ossenkopp, K.-P., and Kavaliers, M. (2021). Sex and age differences in locomotor and anxiety-like behaviors in rats: From adolescence to adulthood. Dev. Psychobiol. *63*, 496–511. https://doi.org/10.1002/dev.22037.

43. Sudakov, S.K., Alekseeva, E.V., Nazarova, G.A., and Bashkatova, V.G. (2021). Age-Related Individual Behavioural Characteristics of Adult Wistar Rats. Animals (Basel) *11*, 2282. https://doi.org/10.3390/ani11082282.

44. Pellis, S.M., and Pellis, V.C. (1991). Attack and Defense During Play Fighting Appear to be Motivationally Independent Behaviors in Muroid Rodents. Psychol. Rec. *41*, 175–184. https://doi.org/10.1007/BF03395104.

45. Burghardt, G.M., Pellis, S.M., Schank, J.C., Smaldino, P.E., Vanderschuren, L.J.M.J., and Palagi, E. (2024). Animal play and evolution: seven timely research issues about enigmatic phenomena. Neurosci. Biobehav. Rev. *160*, 105617. https://doi.org/10.1016/j.neubiorev.2024.105617.

46. SenGupta, P. (2013). The Laboratory Rat: Relating Its Age With Human's. Int. J. Prev. Med. *4*, 624–630.

47. Taylor, G.T., Frechmann, T., and Royalty, J. (1986). Social behaviour and testicular activity of juvenile rats. J. Endocrinol. *110*, 533–537. https://doi.org/10.1677/joe.0.1100533.

48. Meaney, M.J., and McEwen, B.S. (1986). Testosterone implants into the amygdala during the neonatal period masculinize the social play of juvenile female rats. Brain Res. *398*, 324–328. https://doi.org/10.1016/0006-8993(86)91492-7.

49. Tanaka, M., and Sokabe, M. (2013). Bidirectional modulatory effect of 17β-estradiol on NMDA receptors via ERα and ERβ in the dentate gyrus of juvenile male rats. Neuropharmacology *75*, 262–273. https://doi.org/10.1016/j.neuropharm.2013.07.029.

50. Liu, S.B., and Zhao, M.G. (2013). Neuroprotective effect of estrogen: role of nonsynaptic NR2B-containing NMDA receptors. Brain Res. Bull. *93*, 27–31. https://doi.org/10.1016/j.brainresbull.2012.10.004.

51. Cyr, M., Ghribi, O., and Di Paolo, T. (2000). Regional and selective effects of oestradiol and progesterone on NMDA and AMPA receptors in the rat brain. J. Neuroendocrinol. *12*, 445–452. https://doi.org/10.1046/j.1365-2826.2000.00471.x.

52. Achterberg, E.J.M., van Swieten, M.M.H., Houwing, D.J., Trezza, V., and Vanderschuren, L.J.M.J. (2019). Opioid modulation of social play reward in juvenile rats. Neuropharmacology *159*, 107332. https://doi.org/10.1016/j.neuropharm.2018.09.007.

53. Achterberg, E.J.M., and Vanderschuren, L.J.M.J. (2023). The neurobiology of social play behaviour: past, present and future. Neurosci. Biobehav. Rev. *152*, 105319. https://doi.org/10.1016/j.neubiorev.2023.105319.

54. Achterberg, E.J.M., van Kerkhof, L.W.M., Servadio, M., van Swieten, M.M.H., Houwing, D.J., Aalderink, M., Driel, N.V., Trezza, V., and Vanderschuren, L.J.M.J. (2016). Contrasting Roles of Dopamine and Noradrenaline in the Motivational Properties of Social Play Behavior in Rats. Neuropsychopharmacology *41*, 858–868. https://doi.org/10.1038/npp.2015.212.

55. Semple, B.D., Blomgren, K., Gimlin, K., Ferriero, D.M., and Noble-Haeusslein, L.J. (2013). Brain development in rodents and humans: Identifying benchmarks of maturation and vulnerability to injury across species. Prog. Neurobiol. *106–107*, 1–16. https://doi.org/10.1016/j.pneurobio.2013.04.001.

56. Wilton, D.K., Dissing-Olesen, L., and Stevens, B. (2019). Neuron-Glia Signaling in Synapse Elimination. Annu. Rev. Neurosci. *42*, 107–127. https://doi.org/10.1146/annurev-neuro-070918-050306.

57. Kittl, M., Dobias, H., Beyreis, M., Kiesslich, T., Mayr, C., Gaisberger, M., Ritter, M., Kerschbaum, H.H., and Jakab, M. (2018). Glycine Induces Migration of Microglial BV-2 Cells via SNAT-Mediated Cell Swelling. Cell. Physiol. Biochem. *50*, 1460–1473. https://doi.org/10.1159/000494646.

58. Komm, B., Beyreis, M., Kittl, M., Jakab, M., Ritter, M., and Kerschbaum, H.H. (2014). Glycine modulates membrane potential, cell volume, and phagocytosis in murine microglia. Amino Acids *46*, 1907–1917. https://doi.org/10.1007/s00726-014-1745-8.

59. Neniskyte, U., and Gross, C.T. (2017). Errant gardeners: glial-cell-dependent synaptic pruning and neurodevelopmental disorders. Nat. Rev. Neurosci. *18*, 658–670. https://doi.org/10.1038/nrn.2017.110.

60. Zoicas, I., and Kornhuber, J. (2019). The Role of the N-Methyl-D-Aspartate Receptors in Social Behavior in Rodents. Int. J. Mol. Sci. *20*, 5599. https://doi.org/10.3390/ijms20225599.

61. Di Cosmo, A., Di Cristo, C., and Messenger, J.B. (2006). L-glutamate and its ionotropic receptors in the nervous system of cephalopods. Curr. Neuropharmacol. *4*, 305–312. https://doi.org/10.2174/157015906778520809.

62. Chiang, A.-S., Lin, W.-Y., Liu, H.-P., Pszczolkowski, M.A., Fu, T.-F., Chiu, S.-L., and Holbrook, G.L. (2002). Insect NMDA receptors mediate juvenile hormone biosynthesis. Proc. Natl. Acad. Sci. USA *99*, 37–42. https://doi.org/10.1073/pnas.012318899.

63. Burgdorf, J., Moskal, J.R., Brudzynski, S.M., and Panksepp, J. (2013). Rats selectively bred for low levels of play-induced 50 kHz vocalizations as a model for autism spectrum disorders: a role for NMDA receptors. Behav. Brain Res. *251*, 18–24. https://doi.org/10.1016/j.bbr.2013.04.022.

64. Moskal, J.R., Burgdorf, J., Kroes, R.A., Brudzynski, S.M., and Panksepp, J. (2011). A novel NMDA receptor glycine-site partial agonist, GLYX-13, has therapeutic potential for the treatment of autism. Neurosci. Biobehav. Rev. *35*, 1982–1988. https://doi.org/10.1016/j.neubiorev.2011.06.006.

65. Burgdorf, J.S., Zhang, X.-L., Stanton, P.K., Moskal, J.R., and Donello, J.E. (2022). Zelquistinel Is an Orally Bioavailable Novel NMDA Receptor Allosteric Modulator That Exhibits Rapid and Sustained Antidepressant-Like Effects. Int. J. Neuropsychopharmacol. *25*, 979–991. https://doi.org/10.1093/ijnp/pyac043.

66. Bruce, M.R., Couch, A.C.M., Grant, S., McLellan, J., Ku, K., Chang, C., Bachman, A., Matson, M., Berman, R.F., Maddock, R.J., et al. (2023). Altered behavior, brain structure, and neurometabolites in a rat model of autism-specific maternal autoantibody exposure. Mol. Psychiatry *28*, 2136–2147. https://doi.org/10.1038/s41380-023-02020-3.

67. Román, V., Adham, N., Foley, A.G., Hanratty, L., Farkas, B., Lendvai, B., and Kiss, B. (2021). Cariprazine alleviates core behavioral deficits in the prenatal valproic acid exposure model of autism spectrum disorder. Psychopharmacol. (Berl.) *238*, 2381–2392. https://doi.org/10.1007/s00213-021-05851-6.

68. Malkesman, O., Braw, Y., Maayan, R., Weizman, A., Overstreet, D.H., Shabat-Simon, M., Kesner, Y., Touati-Werner, D., Yadid, G., and Weller, A. (2006). Two different putative genetic animal models of childhood depression. Biol. Psychiatry *59*, 17–23. https://doi.org/10.1016/j.biopsych.2005.05.039.

69. Burgdorf, J., Colechio, E.M., Stanton, P., and Panksepp, J. (2017). Positive Emotional Learning Induces Resilience to Depression: A Role for NMDA Receptor-mediated Synaptic Plasticity. Curr. Neuropharmacol. *15*, 3–10. https://doi.org/10.2174/1570159x14666160422110344.

70. Huizinga, J. (1938). Homo Ludens (Routledge & Kegan Paul).

71. Schneider, C.A., Rasband, W.S., and Eliceiri, K.W. (2012). NIH Image to ImageJ: 25 years of image analysis. Nat. Methods *9*, 671–675. https://doi.org/10.1038/nmeth.2089.

72. Henneberger, C., Jüttner, R., Rothe, T., and Grantyn, R. (2002). Postsynaptic action of BDNF on GABAergic synaptic transmission in the superficial layers of the mouse superior colliculus. J. Neurophysiol. *88*, 595–603. https://doi.org/10.1152/jn.2002.88.2.595.

73. Tschida, K., Michael, V., Takatoh, J., Han, B.-X., Zhao, S., Sakurai, K., Mooney, R., and Wang, F. (2019). A Specialized Neural Circuit Gates Social Vocalizations in the Mouse. Neuron *103*, 459–472.e4. https://doi.org/10.1016/j.neuron.2019.05.025.

74. Paxinos, G., and Watson, C. (2007). The Rat Brain in Stereotaxic Coordinates, Sixth Edition (Academic Press).

75. Poole, E.I., McGavin, J.J., Cochkanoff, N.L., and Crosby, K.M. (2019). Stereotaxic surgery for implantation of guide cannulas for microinjection into the dorsomedial hypothalamus in young rats. MethodsX *6*, 1652–1659. https://doi.org/10.1016/j.mex.2019.07.005.

76. de Menezes, R.C.A., Zaretsky, D.V., Fontes, M.A.P., and DiMicco, J.A. (2006). Microinjection of muscimol into caudal periaqueductal gray lowers body temperature and attenuates increases in temperature and activity evoked from the dorsomedial hypothalamus. Brain Research *1092*, 129–137. https://doi.org/10.1016/j.brainres.2006.03.080.

77. Kazanskaya, R.B., Lopachev, A.V., Fedorova, T.N., Gainetdinov, R.R., and Volnova, A.B. (2020). A low-cost and customizable alternative for commercial implantable cannula for intracerebral administration in mice. HardwareX *8*, e00120. https://doi.org/10.1016/j.ohx.2020.e00120.

78. Schneggenburger, R., Meyer, A.C., and Neher, E. (1999). Released fraction and total size of a pool of immediately available transmitter quanta at a calyx synapse. Neuron *23*, 399–409. https://doi.org/10.1016/s0896-6273(00)80789-8.

79. Lu, T., and Trussell, L.O. (2000). Inhibitory transmission mediated by asynchronous transmitter release. Neuron *26*, 683–694. https://doi.org/10.1016/s0896-6273(00)81204-0.

80. Kirischuk, S., and Grantyn, R. (2003). Intraterminal Ca2+ concentration and asynchronous transmitter release at single GABAergic boutons in rat collicular cultures. J. Physiol. *548*, 753–764. https://doi.org/10.1113/jphysiol.2002.037036.

81. Aarts, E., Verhage, M., Veenvliet, J.V., Dolan, C.V., and van der Sluis, S. (2014). A solution to dependency: using multilevel analysis to accommodate nested data. Nat. Neurosci. *17*, 491–496. https://doi.org/10.1038/nn.3648.

Please cite this article in press as: Dvorzhak et al., Social play behavior is driven by glycine-dependent mechanisms, Current Biology (2024), https://doi.org/10.1016/j.cub.2024.06.073

STAR★METHODS

KEY RESOURCES TABLE

REAGENT or RESOURCE	SOURCE	IDENTIFIER
Antibodies		
Rabbit anti-Glycine	Abcam	Cat# ab9442; RRID: AB_1652480
Mouse anti-NeuN	Millipore	Cat# MAB377; RRID: AB_2298772
Guinea pig anti-GABA	Abcam	Cat# ab17413; RRID: AB_443865
Rabbit anti-Glutaminase	Abcam	Cat# ab202027; RRID: AB_3101817
Anti-guinea pig Alexa Fluor 488	ThermoFisher	Cat# A-11073; RRID: AB_2534117
Anti-rabbit Alexa Fluor 488	ThermoFisher	Cat# A-11034; RRID: AB_2576217
Anti-rabbit Alexa Fluor 555	ThermoFisher	Cat# A-21429; RRID: AB_2535850
Anti-mouse Alexa Fluor 647	ThermoFisher	Cat# A-21235; RRID: AB_2535804
Bacterial and virus strains		
AAV2/9-hSyn-WiChR-mScarlet	Vierock et al.[22] Viral Core Facility (VCF) of the Charité-Universitätsmedizin Berlin	RRID: Addgene_205997
Chemicals, peptides, and recombinant proteins		
6,7-dinitroquinoxaline-2,3-dione	Tocris	Cat# 2312
MK-801 maleate	Tocris	Cat# 0924
APV	Abcam	Cat# ab120271
Bicuculline methiodide	Tocris	Cat# 0130
ALX-5407	Tocris	Cat# 1757
HA-966	Tocris	Cat# 0281
Strychnin	Merck/Sigma-Aldrich	Cat# S0532
Tetrodotoxin (TTX)	Abcam	Cat# ab120054
Muscimol	Abcam	Cat# ab120094
DiI (1,10-Dioctadecyl-3,3,30,30-tetramethylindocarbocyanine perchlorate)	Merck/Sigma-Aldrich	Cat# 42364
Lidocain-HCl 2%	B.Braun	N/A
0.9% NaCl for injections	B.Braun	N/A
Metamizol	Ratiopharm GmbH, Ulm, Germany	N/A
Eye cream Bepanten, Bayer	Medios Apotheke an der Charte, Luisenstraße 54/55, 10117, Berlin, Germany	N/A
Carprofen / (Carprosol)	CP-Pharma	Cat# 115
Sodium Chloride NaCl	Carl Roth GmbH	Cat# P029.5
Sodium Carbonate Na_2CO_3	Carl Roth GmbH	Cat# P028.1
Sodium Pyruvate $CH_3COCOONa$	Carl Roth GmbH	Cat# 8793.1
Sodium Ascorbate	Merck/Sigma-Aldrich	Cat# PHR1279
Sodium dihydrogen phosphate NaH_2PO_4	Carl Roth GmbH	Cat# T879.1
Sodium Gluconate	Merck/Sigma-Aldrich	Cat# S2054
Sodium GTP	Merck/Sigma-Aldrich	Cat# 51120
Potassium Chloride KCl	Merck/Sigma-Aldrich	Cat# P5405
Potassium Gluconate	Merck/Sigma-Aldrich	Cat# P1847
Potassium Hydroxid KOH	Carl Roth GmbH	Cat# P747.1
Magnesium Chloride Hexahydrate $MgCl2*6H_20$	Carl Roth GmbH	Cat# 2189.2
Magnesium ATP	Merck/Sigma-Aldrich	Cat# A9187
Calcium Chloride Dihydrate $CaCl_2$-$2H_20$	Carl Roth GmbH	Cat# HN04.1
Cholinchlorid	Merck/Sigma-Aldrich	Cat# C1879
Glucose	Merck/Sigma-Aldrich	Cat# HN06.3

(*Continued on next page*)

Please cite this article in press as: Dvorzhak et al., Social play behavior is driven by glycine-dependent mechanisms, Current Biology (2024), https://doi.org/10.1016/j.cub.2024.06.073

Continued

REAGENT or RESOURCE	SOURCE	IDENTIFIER
Cesium methanesulfonate Cs-CH3SO3	Merck/Sigma-Aldrich	Cat# C1426
Cesium chloride CsCl	Merck/Sigma-Aldrich	Cat# C4036
Cesium Hydroxid Hydrat CsOH*H2O	Merck/Sigma-Aldrich	Cat# C8518
EGTA	Merck/Sigma-Aldrich	Cat# E4378
HEPES	Carl Roth GmbH	Cat# 9105.4
Alexa-594	ThermoFisher	Cat# A10438
Agarose	Carl Roth GmbH	Cat# 3810.2
Fluorshield - DAPI	Merck/Sigma-Aldrich	N/A
Super Glue	UHU GmbH & Co. KG Bühl/Baden, Germany	N/A
Paladur	Kulzer GmbH, Germany	N/A
Experimental models: Organisms/strains		
Long-Evans Rats	Janvier Labs	N/A
Software and algorithms		
ImageJ 1.47q	Schneider et al.[71]	RRID: SCR_003070
RStudio 2022.02.3 Build 492	Posit	RRID: SCR_000432
GraphPad Prism 8	GraphPad	RRID: SCR_002798
Anaconda with Python 3.7.4	Anaconda Inc.	RRID: SCR_008394
Leica Application Suite X	Leica Microsystems	RRID: SCR_013673
WinWCP	Strathclyde University	RRID: SCR_014713
Tida v4.11	HEKA Elektronik	RRID: SCR_014582
Corel Graphics Suite	CorelDRAW	RRID: SCR_013674
Mendeley	Elsevier	RRID: SCR_002750
DeepLabCut	MMathisLab	RRID: SCR_021391
PeakCount v 3.2	Hennenberger et al.[72]	N/A
Microsoft Office	Microsoft	N/A
Other		
Guide cannulas, G26 needles, Sterican	B.Braun	Cat# 4657683
Injection cannulas for substances	World Percision Instruments	Cat# NF33BV-2
Injection cannulas, for viruses	World Percision Instruments	Cat# NF34BV-2
Syringe, Nanofil 10 μl	World Percision Instruments	Cat# NANOFIL
Blue LEDs	Kingbright	Cat# APG0603VBC-A1-5MAV
PLA plastic for 3D-printing	Verbatim	Cat# 55904

RESOURCE AVAILABILITY

Lead contact

Further information and requests for resources and reagents should be directed to and will be fulfilled by the lead contact, Dietmar Schmitz (dietmar.schmitz@charite.de).

Materials availability

This study did not generate new unique reagents.

Data and code availability

This study did not generate any unique datasets or code. All data on figures with detailed statistical analysis are available in Data S1. Any additional information required to reanalyze the data reported in this paper is available from the lead contact upon request.

EXPERIMENTAL MODEL AND STUDY PARTICIPANT DETAILS

Animal maintenance and experiments were in accordance with the respective guidelines of local authorities and approved by the state government of Berlin (LAGESO, licenses: T0073/04, G0072/21) as well as followed the German animal welfare act and the European Council Directive 2010/63/EU on protection of animals used for experimental and other scientific purposes.

5-week-old male C57BL/6NRj mice, 4-6 (juvenile) and 20-30 (adult) week-old male Long-Evans rats were provided by Janvier Labs at 3 weeks of age. Rats were kept in pairs in 59 cm x 38 cm x 26 cm cages filled with wooden chips and containing thin papers, plastic shelters (usually pipes) and a wooden bar. Animals had permanent access to food and water and were maintained at 22 ^{0}C with a 12/12 hour light/dark cycle (lights on at 6 am).

The required number of animals determination for behavioral experiments was based on the publication[73] using a two-tailed paired t-test assuming of significance level $\alpha = 0,05$, power (1-β) = 80% and 20% drop outs, as well as approved by the state government of Berlin (LAGESO, licenses: G0072/21).

METHOD DETAILS

Surgery

Surgery was performed on 3-4 weeks old juvenile (weight 60-80 g) and 20-23 weeks old adult (330-400 g) rats under isoflurane (1.5% in oxygen) anesthesia. To prevent post-operative pain and inflammation, the rats were given metamizole dissolved in drinking water (200 mg/kg body weight) the day before and three days after the operation and carprofen (5mg/kg body weight) was injected subcutaneously 30 min before the operation. As an additional pain killer, 2% lidocaine was injected locally subcutaneously. Since in juvenile rats the distance between the bregma and the interaural line varies from 7.2 to 8.1 mm, stereotactic coordinates taken from the atlas[74] for adult rats, where this parameter is 9 mm, were scaled proportionally for each animal individually. The non-scaled coordinates are given in mm relative to bregma.

All animals that successfully survived postoperative recovery (1 week for deep brain injections, 2 weeks for optogenetics) and showed daily weight gain were used for behavioral experiments.

Implantation of guide cannulas and deep brain injections

The following publications were used as a basis for developing the surgery protocol.[75–77] Sharpened G26 needle tips (7 mm long) were used as guiding cannulas. On the blunt side, 1 cm polyethylene tubing was glued to the cannulas as required for positioning, protection against bacterial contamination of the cannulas and to simplify the insertion of the injection cannula. After sterilization with 100% EtOH overnight guide cannulas were implanted bilaterally at a 9° angle to the vertical (in the coronal plane) to prevent damage to the superior sagital sinus and glandula pineale. The stereotactic coordinates for implantation (relative to Bregma: anteroposterior (AP) -7.68, mediolateral (ML) 1.63; relative to dura mater: dorsoventral (DV) 2.46) were chosen so that the injection cannula would hit the PAG, while the guiding cannula would not touch it (Figure 1D). After implantation, the guide cannulas were fixed with acrylic glue and the polyethylene tubing was sealed. For better fixation of the cannulas, a 3D-printed plastic ring with an external thread (internal diameter = 7 mm, external diameter = 1 0 mm, height = 4 mm) was glued. The entire interior space of the ring was then filled with Hoffmann's dental phosphate cement pasta. At the end a plastic cap (height = 11 mm) was put on the ring and additionally secured with a screw to cover the cannulas with polyethylene tubes from the rats' paws. After a one-week recovery period, the day before the experiment, the rat's cap was removed, the polyethylene tubes were cut and a control isotonic 0.9% NaCl solution was injected with a Hamilton syringe and 33 Ga x 10 mm needle (NanoFil #NF33BV) through guiding cannulas, 2 μl into each hemisphere. This pre-injection helps to reduce the suppression of play by the increased stress of the very first injection. In general, the bilateral deep brain injection procedure lasts between 30 sec and 1 min and does not induce visible motor disturbances or behavioral abnormalities, but suppresses playfulness by 30%. The distribution of the injected substances in the PAG was assessed by the distribution of the green dye DiR injected postmortem (Figure 1E).

Optogenetics

For optogenetic suppression of play behavior, rats were bilaterally injected with AAV2/9-hSyn-WiChR-mScarlet[22] (2x10^{12}VG/ml) in PAG by portions of 1 μL per injection, 2 injections per hemisphere. Injection velocity was 0.2 μl/min. The injection needle (NanoFil #NF34BV) was angled 9° to the vertical and positioned at the following coordinates: injection 1 – AP = -7.68, ML = 1.63, DV = 5.46; injection 2 – AP = -7.68, ML = 1.48, DV = 4.47 (Figure 1H).

For further optical activation of the WiChR[22] construct, 470 nm blue LEDs (0.65 mm x 0.35 mm x 0.2 mm 0402 SMD chip Kingbright APG0603VBC-A1-5MAV) were bilaterally implanted immediately after the injections in a vertical manner (AP = -7.68, ML = 2, DV = 5.5; Figure 1H). The blue light from the LEDs (16 mW) was completely absorbed by the 2 mm white and 3 mm grey matter of the brain. The LEDs were soldered to copper wires (diameter 50 μm) coated with lacquer and placed inside a polyethylene tube with a diameter of 250 μm. The contact points were electrically insulated from the environment with cyanoacrylate glue. The wires connected the LEDs to a self-made wireless Bluetooth device, which was encapsulated in a 3D-printed housing (with maximum dimensions of 21 mm x17 mm x13 mm) together with the battery (CR1632), that continuously powered the device for over 5 hours. The Bluetooth device (JDY-16) was attached to the skull by a printed plastic ring that was separately glued to the skull. To ensure the fixation of the optical stimulator the inner space of the fixation ring with screws and LEDs wires was completely filled with Hoffmann's phosphate cement. The one-week recovery period was also sufficient for the expression of WiChR, whose distribution in PAG as well as location of LEDs were checked in postmortem histology. The LEDs were controlled remotely via a smartphone using a self-made program. Optical activation of the WiChR was carried out with constant blue light bilaterally for 2 minutes.

Please cite this article in press as: Dvorzhak et al., Social play behavior is driven by glycine-dependent mechanisms, Current Biology (2024), https://doi.org/10.1016/j.cub.2024.06.073

Behavior

Assessment of rough-and-tumble play (RTP) in male Long-Evans rats aged 4-6 or 25-30 weeks was based on the protocol of VanRyzin et al.[18] and conducted during the light phase of a 12:12 h reverse light:dark cycle, but in the dark using 750 nm infrared illumination (IR). The open plexiglass cage with dimensions of 55 cm x 37 cm x 50 cm was placed in a large non-transparent container (131 cm x 96 cm x 81 cm) and partially filled with wood bedding (2-3 cm). The video recording of the RTP was done using a Raspberry Pi camera (OV5647) connected to Raspberry Pi A and located with 2 IR- LEDs approximately 1 m above the playing arena (Figure 1A2). The videos were acquired using internal commands of the Raspbian GNU/Linux 10 (buster) operating system (Cambridge, UK). To habituate the rats to the experimental conditions, starting two days before the experiment, the animals were individually placed for at least 10 min every day on a play arena under experimental conditions. To increase the frequency of RTP, rats were placed in single cages 24 hours before the experiment. For darkness habituation, rats were placed in a dark experimental room for at least 20 min before the experiment and during habituation. The experiment always started with a 10-minute open field test on the play arena followed by a 3 min rest in a home cage, after that a pair of rats was put together to observe RTP. The rats were given approximately 1 min to acclimate before video recording started. After 5 or 10 min (depending on the type of experiment) of RTP video recording, the rats were returned to their home cage. The test rat (injected or with activated LEDs) was returned to the playing arena after a 3 min rest for the 10 min open field test, while the other rat (CTRL) remained in its cage until the next playing session. Control experiments showed that this protocol reduces the RTP playfulness by 50% in CTRL rats after 3 or 4 five-minute lasting RTP cycles, while in test rats we saw this reduction after 4-5 cycles (data not shown).

Behavior was scored offline by an experimenter and his children randomly and blind to the experimental conditions. A detailed definition and video of behavioral events can be found in the corresponding bio-protocol of VanRyzin et al.[18] To assess rat playfulness, each video was viewed frame-by-frame and the beginning and end of the playful event (pinning, pouncing and boxing) were registered. The RTP playfulness was defined as the percentage of the cumulative duration of pouncing, pinning and boxing events relative to the total video recording time. When comparing RTP scoring under control conditions (isotonic NaCl injections) there is no significant difference between RTP assessors (2w-ANOVA $F(3,57)=0.09$, $p=0.96$, Figure S1I), while there is a difference between CTRL and injected rats (2w-ANOVA $F(1,57)=4.69$, $p=0.03$, Figure S1I). There is also no statistical interaction between assessors and rat type (2w-ANOVA $F(3,57)=1.25$, $p=0.3$, Figure S1I). The 10-min pathway in the open field test was measured by tracking rats using DeepLabCut.

Electrophysiology

Slices preparation

Rats (P23-41, males) were decapitated following isoflurane anesthesia. Brains were removed and transferred to ice-cold, choline-based artificial cerebrospinal fluid (chACSF) containing (in mM) 125 Choline-Cl, 2.5 KCl, 1.25 NaH2PO4, 25 NaHCO3, 10 Glucose, 0.5 CaCl2, 7 MgCl2, 0.5 Na-Pyruvate, 2.8 Na-Ascorbat, saturated with 95% O_2, 5% CO_2, pH 7.4 and adjusted to osmolarity 302 mosmol/l with water. Slices (300 μm) were cut in a coronal plane on a vibratome (VT1200S; Leica) and stored in a submerged chamber filled with chACSF at room temperature continuously oxygenized with carbogen. After 30 min of incubation in chACSF slices were transferred to a chamber with artificial cerebrospinal fluid (ACSF) containing (in mM) 126 NaCl, 25 $NaHCO_3$, 11 glucose, 2.5 KCl, 2.4 $CaCl_2$, 1.2 $MgCl_2$, 1.4 NaH_2PO_4. The equilibration time was at least 1 hour after preparation before they were transferred to the recording chamber.

Patch-clamp recording

Recordings were performed in ACSF at 32-34°C in a submerged-type recording chamber. Cells in the PAG were identified using infrared differential contrast microscopy (BX51WI, Olympus). A Femto2D 2-photon laser scanning system (Femtonics, Budapest, Hungary) equipped with a femtosecond pulsed Ti:Sapphire laser tuned to $\lambda = 805$ nm and power 0.5W(Cameleon, Coherent, Santa Clara, CA, US) controlled by the MATLAB-based MES software package (Femtonics, Budapest, Hungary) was used to acquire images of fluorophore-filled cells. Fluorescence was acquired in epifluorescence mode with a water immersion objective (LUMPLFL 60×/1.0 NA or UMPlanFL 10×/0.3 NA, Olympus, Hamburg, Germany). Transfluorescence and transmitted infrared were detected using an oil immersion condenser (Olympus).

We performed somatic whole-cell patch-clamp recordings (pipette resistance 2-6 MΩ). In experiments where was used the current-clamp mode the intracellular solution contained (in mM) 155 K-Gluconate, 4 KCl, 5 Na-Gluconate, 0.5 $CaCl_2$, 5 EGTA, 25 HEPES, 2 Mg-ATP, 0.3 Na-GTP. The pH was adjusted to 7.2 with KOH. In experiments where spontaneous postsynaptic currents were analyzed in the voltage-clamp mode the intracellular solution contained (in mM) 155 Cs-CH_3SO_3, 4 CsCl, 5 Na-Gluconate, 0.5 $CaCl_2$, 5 EGTA, 25 HEPES, 2 Mg-ATP 0.3 Na-GTP, 0.03 Alexa-594. The pH was adjusted to 7.2 with CsOH. Recordings were performed using Multiclamp 700A/B amplifiers (Molecular Devices). Signals were filtered at 3 kHz, sampled at 10 kHz and digitized at 16 bit resolution using the Digidata 1550 (Molecular Devices) and WinWCP v5.5.2 (University of Strathclyde Glasgow, UK) or TIDA 4.11 software (HEKA Elektronik, Lambrecht, Germany). The experimentally determined reversal potential of GABA(A)-induced chloride currents (E_{Cl}) was -60 mV. To record excitatory postsynaptic currents (EPSC) in voltage-clamp the holding potential was set to -60 mV, to record inhibitory postsynaptic currents (IPSC) it was set to 0 mV. Only recordings with a series resistance below 20 MΩ were accepted (average series resistance amounted to 11 MΩ). Series resistance compensation was not applied. Access resistance was controlled by regularly (1/60 s) applying hyperpolarizing pulses of 10 mV. Cells exhibiting more than 20% changes in the access resistance during an experiment were discarded. Spontaneous and miniature postsynaptic currents were analyzed using a PeakCount V3.2 (courtesy of Dr Christian Hennenberger). The program employs a derivative threshold-crossing algorithm to detect

Please cite this article in press as: Dvorzhak et al., Social play behavior is driven by glycine-dependent mechanisms, Current Biology (2024), https://doi.org/10.1016/j.cub.2024.06.073

individual PSCs with visual inspection of each event. Spontaneous firing activity of neurons was recorded in current clamp mode at holding current 0 mV.

Electrical stimulation

Evoked glycinergic inhibitory postsynaptic currents (eIPSCs) were elicited by focal electrical stimulation through a glass pipette filled with ACSF (about 10 MΩ) in presence of 20 μM. An isolated stimulation unit (Axon Instruments Isolator-11) was used to generate rectangular electrical pulses with 0.5 ms duration. Pulse intensity was adjusted to activate a unitary synaptic input (minimal stimulation). Stimulation was accepted as minimal if the following criteria were satisfied: (1) eIPSC latency remained stable (<20% fluctuations); (2) lowering stimulus intensity by 20% resulted in a complete failure of eIPSCs; and (3) an increase in stimulus intensity by 20% changed neither mean eIPSC amplitude nor eIPSC shape. Typical pulse intensity required for minimal stimulation was between 1 and 2 μA.

Estimation of readily releasable pool size

To estimate the size of the readily releasable pool (RRP), we used high frequency stimulation.[78–80] Repetitive stimulation leads to a decrease in the eIPSC amplitudes. Assuming that the eIPSC depression is largely caused by a transient decrease in the number of readily releasable quanta, it is possible to estimate the RRP size on the basis of the cumulative eIPSC amplitude plot.[78–80] Namely, stimulation trains of 100 pulses delivered at 40 Hz were applied and cumulative eIPSC amplitudes were plotted versus stimulus number (Figure 3). Because repetitive stimulation causes a compound postsynaptic response (synchronous and asynchronous), PSCs that peaked within a 3 ms interval following the end of a stimulus pulse were selected as stimulus-locked eIPSCs. After 50 pulses, the cumulative eIPSCs reached a steady state, as indicated by the linear slope dependence of the cumulative eIPSC amplitude on the pulse number (Figure 3C). Assuming that (1) the number of release sites remains constant throughout the experiment and (2) the linear component reflects vesicle recycling, the cumulative IPSC amplitude in the absence of pool replenishment can be estimated by back-extrapolation to the start of the train (Y-intercept, Figures 3C and 3D). Note Y-intercept represents the product of the RRP and the quantal amplitude. Since the synapse releases vesicles in a quantal manner after depletion, the size of the RRP is the Y-intercept normalized by the mean amplitude of late eIPSCs, which are defined as synchronous responses to the last 50 stimuli excluding failures (Figures 3D–3F). Indeed, during 40 Hz trains the mean late eIPSC amplitude has been shown to be close to the median miniature IPSC amplitude in this preparation (Figures 2D, 2F, and 3E). It should be mentioned that only late eIPSCs but not asynchronous IPSCs[79] were selected to obtain an estimate of the quantal amplitude for the projection of interest. Release probability (Pr) was calculated using the binomial model approximation, namely, Pr = mean eIPSC-amplitude/RRP/Quantal size.

Pharmacology

The glutamatergic nature of ion currents was verified by applying the AMPA receptor blocker 6,7-dinitroquinoxaline-2,3-dione (DNQX, 10 μM) and the NMDA receptor blocker MK-801 maleate (MK-801, 1 μM) or APV (50 μM). Similarly, the GABA(A) receptor blocker bicuculline methiodide (BMI, 20 μM) was used to block GABAergic currents and strychnine hydrochloride (Str, 2 μM) was used to block glycinergic currents. To test for involvement of GlyT1, we used the non-transportable inhibitor ALX-5407 (1 μM). To test for involvement of the glycine binding site on NMDA receptors, we used HA-966 (400 μM). To block Na^+-channels in slice experiments and record miniature postsynaptic currents, tetrodotoxin (TTX, 1 μM) was used.

Immunohistochemistry

Slices preparation

To prepare slices for immunohistochemical studies the animals were euthanized with Isoflurane and transcardially perfused with 0.9% saline followed by 4% paraformaldehyde (PFA) in PBS. Brains were harvested and immersion-fixed in 4% PFA for 24 h. After fixation, brains were placed in PBS+0.1%NaN3 solution for PFA washing and storage. Brains were cut into 40 μm coronal sections using a vibratome (VT1200S; Leica) and 5% agar block. The free-floating sections were stored in PBS containing 0.1% sodium azide in 24-well cell culture plates at 4 °C.

Staining

The sections were washed 3 × 10 min with 0.1M PBS and incubated at room temperature for 3 h in immunobuffer containing 0.1 M PBS, 1% Triton X-100 (Sigma-Aldrich) and 5% normal goat serum. The primary antibodies were diluted in immunobuffer and applied to the sections for 48 h incubation with light agitation at 4 ^{0}C temperature. The primary antibodies and their dilutions were as follows: rabbit anti-Glycine 1:500, mouse anti-NeuN 1:1000, guinea pig anti-GABA 1:500, rabbit anti-Glutaminase. After incubation, following 2 × 10 min washes in 0.1M PBS, appropriate fluorophore-conjugated secondary antibodies diluted 1:500 in immunobuffer were applied and the sections were incubated for 3 h with light agitation at room temperature. The secondary antibodies were: goat anti-guinea pig Alexa Fluor 488, goat anti-rabbit Alexa Fluor 488, goat anti-rabbit Alexa Fluor 555, goat anti-mouse Alexa Fluor 647. Following incubation with the secondary antibodies, brain tissues were washed 3 × 10 min in PBS, mounted onto glass slides with DAPI containing mountain media (Fluorshield- Dapi; F6057-20ML; Sigma-Aldrich) and covered.

Confocal microscopy

Mounted slices were imaged using a confocal microscope (Leica DMI 6000), equipped with a 20x immersion objective (HC PL APO 20x/0.70 IMM). Images were acquired with the LAS X 3.1.5.16308 software (Leica Microsystems, Germany). A 405 nm diode was used to excite DAPI, a 488 nm OPSL laser was used to excite Alexa Fluor 488, a 552 nm OPSL laser was used for Alexa Fluor 555 or mScarlet, and a 638 nm diode was used for Alexa Fluor 647. Emission was detected by 4 photomultiplier tubes: 410-530 nm for DAPI, 497-577 nm

Please cite this article in press as: Dvorzhak et al., Social play behavior is driven by glycine-dependent mechanisms, Current Biology (2024), https://doi.org/10.1016/j.cub.2024.06.073

for Alexa Fluor 488, 560-630 nm for Alexa Fluor 555 and 650-750 nm for Alexa Fluor 647. The pinhole was 60.5 μm. Laser power and gain were kept the same for all imaged slices and conditions. Each image was acquired by averaging of 3 frames, where each line was an average result of 2 scan lines. Each image channel was acquired independently of each other. The final slice image was obtained by stitching together and aligning the brightness of the individual square fragments.

QUANTIFICATION AND STATISTICAL ANALYSIS

The results are presented as mean ± S.E.M. In all figures the error bars indicate that the S.E.M. normality of the data distributions was assessed using the Kolmogorov–Smirnov test (KS-t). Considering that the comparison of means could be influenced by inter-animal variance in slice experiments,[81] we performed multilevel (“nested data”) analysis, when necessary. Differences between means were determined by the nested t-test (nested t-t), Student’s paired t-test (pt-t) or its corresponding non-parametric analog (Wilcoxon matched-pairs signed rank test, W-t), and the unpaired non-parametric Mann-Whitney test (MW-t), as appropriate. Differences between groups were tested using one-way repeated measures ANOVA summary (1-way-RM-ANOVA) or an equivalent non-parametric method (Friedman test), followed by a multiple comparison corrected Tukey’s test (Tukey-MCT) or a corresponding non-parametric method (Dunn’s-MCT). All statistical tests used are two-sided. All data points in the figures connected by straight gray lines represent paired measurements made on the same rat or cell. P values of <0.05 were considered statistically significant. Significance levels were marked by asterisks, as follows: *-p<0.05, **-p<0.01, and ***-p<0.001. The abbreviation “ns” in the figures means “not significant”. Cohen’s d ("d" in the figures) $= |Mean_2 - Mean_1| / \sqrt{(SD_1{}^2 * (n_1 - 1) + SD_2{}^2 * (n_2 - 1))/(n_1 + n_2 - 2)}$ was used to estimate effect sizes. In figures describing electrophysiological or immunohistochemical experiments, the numbers on the bars in the numerator indicate the number of measured units (slices or cells, as indicated in figure legends or tables), and in the denominator the number of groups (animals). In figures describing behavioral experiments the numbers on the bars show the number of used animals. Each behavioral experiment was performed with each rat only once.

Current Biology, Volume *34*

Supplemental Information

Social play behavior is driven by glycine-dependent mechanisms

Anton Dvorzhak, Michael Brecht, and Dietmar Schmitz

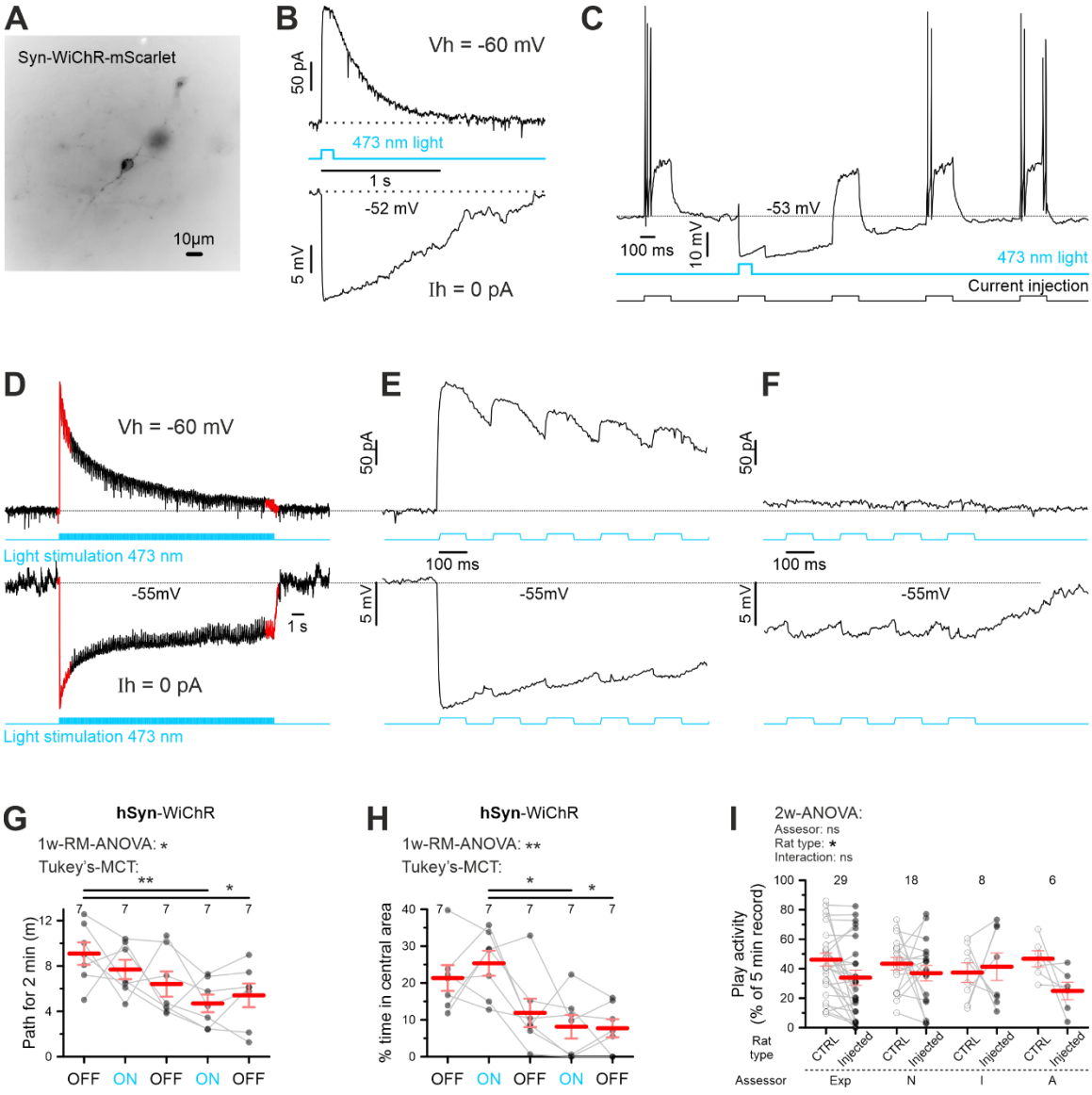

Figure S1. Optogenetic inhibition of PAG neurons by WiChR and its effects in open-field test. Related to Figure 1 and STAR Methods.

A. Dorso-lateral PAG slice image showing expression of Syn-WiChR-mScarlet construct one week after viral injection. **B.** Example traces of membrane currents (top) and potentials (bottom) recorded in dlPAG-neuron in response to a 100 ms pulse of 473 nm light. **C.** Example trace of membrane potentials showing prolong suppression of neuronal firing by a 473 nm light pulse. **D.** Example traces of membrane currents (top) and potentials (bottom) showing inhibition of the dlPAG neuron for 1 min by 300 pulses of 473 nm light applied at 5Hz. The same stimulation protocol was used in optogenetic experiments in vivo. Red marks elements of the traces enlarged in E, F. **E-F.** The enlarged initial (**E**) and final (**F**)

fragments of the stimulation shown in D. **G-H.** The results of open-field tests for rats expressing WiChR in all neurons show no significant change between different phases of illumination, but demonstrate a monotonic change over the course of the experiment. **G**) The statistics of the 2 min path, WiChR in all neurons. 1w-RM-ANOVA: $F(2.33, 13.97) = 4.56$, $p = 0.03$. **H**) The statistics of the % time in central area, WiChR in all neurons. 1w-RM-ANOVA: $F(2.52, 15.12) = 6.48$, $p = 0.007$. **I.** Comparison of play activity scoring under control conditions (isotonic NaCl injections in PAG) between different assessors for injected rats and its play partner (CTRL rats).

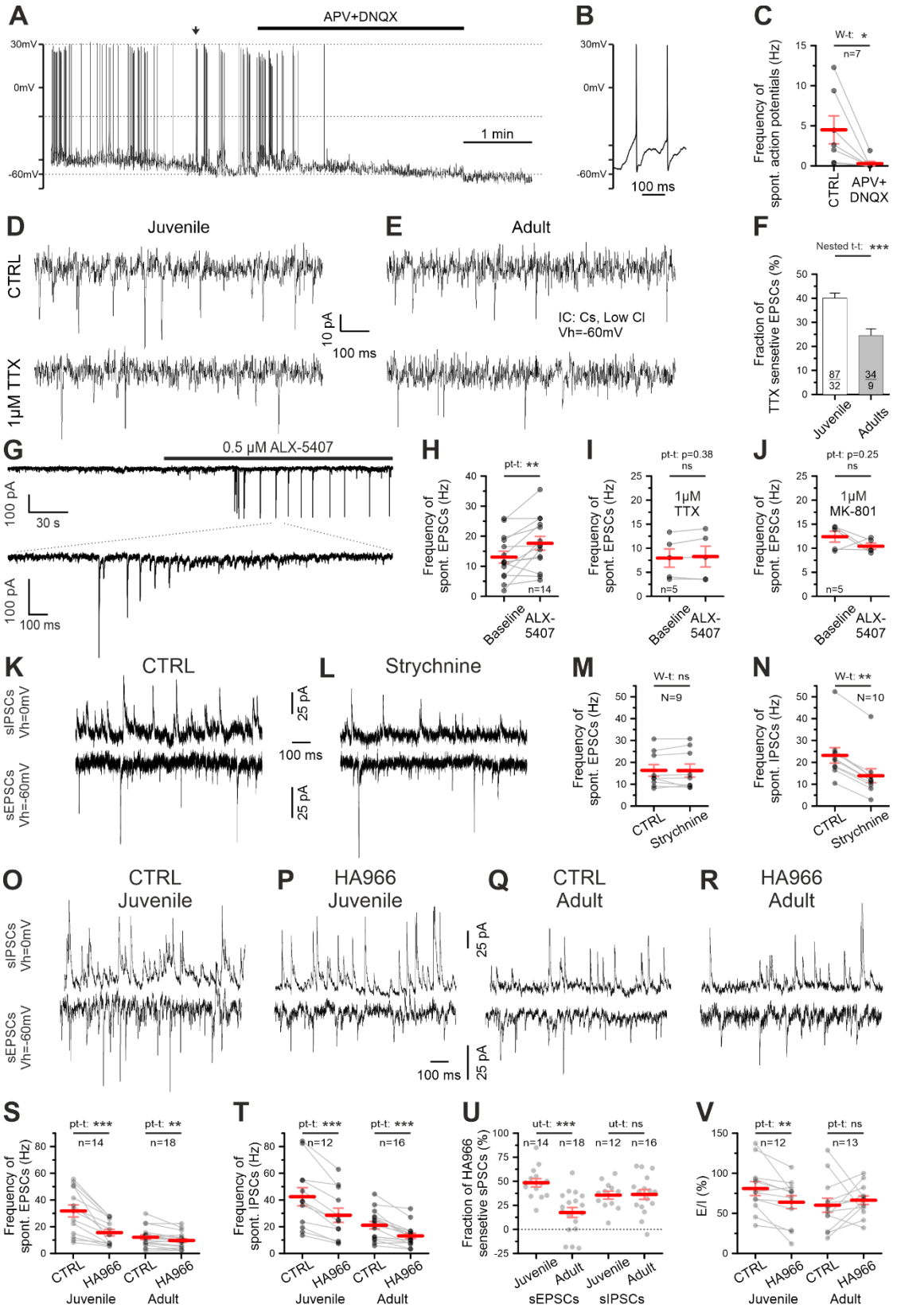
A
APV+DNQX
30mV
0mV
-60mV
1 min
B
30mV
0mV
-60mV
100 ms
C
W-t: *
n=7
Frequency of spont. action potentials (Hz)
CTRL
APV+ DNQX
D
Juvenile
CTRL
1µM TTX
10 pA
100 ms
E
Adult
IC: Cs, Low Cl
Vh=-60mV
F
Nested t-t: ***
Fraction of TTX sensetive EPSCs (%)
87
32
34
9
Juvenile
Adults
G
0.5 µM ALX-5407
100 pA
30 s
100 pA
100 ms
H
pt-t: **
Frequency of spont. EPSCs (Hz)
n=14
Baseline
ALX-5407
I
pt-t: p=0.38
ns
1µM TTX
Frequency of spont. EPSCs (Hz)
n=5
Baseline
ALX-5407
J
pt-t: p=0.25
ns
1µM MK-801
Frequency of spont. EPSCs (Hz)
n=5
Baseline
ALX-5407
K
CTRL
sIPSCs Vh=0mV
sEPSCs Vh=-60mV
25 pA
100 ms
25 pA
L
Strychnine
M
W-t: ns
N=9
Frequency of spont. EPSCs (Hz)
CTRL
Strychnine
N
W-t: **
N=10
Frequency of spont. IPSCs (Hz)
CTRL
Strychnine
O
CTRL Juvenile
sIPSCs Vh=0mV
sEPSCs Vh=-60mV
P
HA966 Juvenile
Q
CTRL Adult
25 pA
100 ms
25 pA
R
HA966 Adult
S
pt-t: ***
n=14
pt-t: **
n=18
Frequency of spont. EPSCs (Hz)
CTRL
HA966
CTRL
HA966
Juvenile
Adult
T
pt-t: ***
n=12
pt-t: ***
n=16
Frequency of spont. IPSCs (Hz)
CTRL
HA966
CTRL
HA966
Juvenile
Adult
U
ut-t: ***
n=14
n=18
ut-t: ns
n=12
n=16
Fraction of HA966 sensetive sPSCs (%)
Juvenile
Adult
Juvenile
Adult
sEPSCs
sIPSCs
V
pt-t: **
n=12
pt-t: ns
n=13
E/I (%)
CTRL
HA966
CTRL
HA966
Juvenile
Adult

Figure S2. Spontaneous neuronal and synaptic activity in PAG neurons. Related to Figure 2.

A. Trace of postsynaptic potentials recorded with CC-mode (at $I_{holding}$ = 0 pA) using K-based intracellular pipette solution in neurons from a caudal dl-PAG young rat slice before, during and after application of 50 μM APV + 10 μM DNQX. Note the complete block of neuronal firing after application of ionotropic Glu-receptors blockers. **B.** Traces of two action potentials marked with an arrow in panel A. **C.** Statistics of action potential (AP) frequency counted during the 1 min period before and at the end of APV+DNQX application shows complete suppression of neuronal firing by blockers of ionotropic glutamate receptors. Wilcoxon sum of signed ranks (W) = -28, p = 0.02, Cohen's d = 1.3. **D-E.** Traces of sEPSCs under control conditions (CTRL, top traces) and in the presence of 1 μM TTX (bottom traces) recorded with low-Cl (5mM) intracellular pipette solution in VC-mode ($V_{holding}$= -60 mV) in dlPAG neurons from juvenile (**D**) and adult rats (**E**). **F.** The fraction of TTX sensitive EPSCs show a significant age-dependent decrease. For nested t-test: t = 3.95, df = 39, F(1,39) = 15.58, p = 0.0003, Cohen's d = 0.93. **G.** Trace of sEPSCs recorded in dlPAG neuron from juvenile rat slice before and after application of the GlyT1 inhibitor 0.5 μM ALX-5407 (upper trace). At the bottom is an enlarged fragment of the burst triggered by the ALX-5407 application. **H.** Frequency of sEPSCs recorded before and after ALX-5407 application show a temporal increase in the activity of excitatory inputs in response to the application. t = 3.24, df = 13, p = 0.007, Cohen's d = 0.58. **I.** Blockade of Na+-channels with 1 μM TTX completely blocks the effect of ALX-5407 on the frequency of spontaneous EPSCs. t = 0.99, df = 4, p = 0.38. **J.** Blockade of NMDA-receptors with 1 μM MK-801 completely blocks the effect of ALX-5407 on the frequency of sEPSCs. t = 1.35, df = 4, p = 0.25. **K-L.** Traces of sPSCs under control conditions (**K**) and in the presence of 2 μM strychnine (**L**) recorded with the same pipette solution as in D-E at $V_{holding}$= 0 mV to detect sIPSCs (upper traces) and at $V_{holding}$= -60 mV to detect sEPSCs (lower traces) in dlPAG neurons from juvenile rats. **M.** 2μM strychnine doesn't change sEPSCs frequency. Wilcoxon test: p = 0.82, Sum of signed ranks = 5. **N.** 2μM strychnine reduces sIPSCs frequency. Wilcoxon test: p = 0.002, Sum of signed ranks = 55. **O-R.** Traces of sPSCs under control conditions (**O, Q**) and in the presence of 200 μM HA966 (**P, R**) recorded with the same pipette solution as in D-E at $V_{holding}$= 0 mV to detect sIPSCs (upper traces) and at $V_{holding}$= -60 mV to detect sEPSCs (lower traces) in dlPAG neurons from juvenile (**O, P**) and adult (**Q, R**) rats. **S.** 200μM HA966 reduces sEPSCs frequency in juvenile (t = 5.4, df = 13, p = 0.0001) and adult (t = 3.6, df = 17, p = 0.002) rats. **T.** 200μM HA966 reduces sIPSCs frequency in juvenile (t = 5.7, df = 11, p = 0.0001) and adult (t = 5.3, df = 15, p < 0.0001) rats. **U.** The fraction of HA966 sensitive sEPSCs shows a significant age dependency (t = 4.4, df = 30, p = 0.0001), whereas the fraction of HA966 sensitive sIPSCs is age independent (t = 0.1, df = 26, p = 0.91). **V.** HA966 decreases E/I only in juvenile (t = 3.2, df = 11, p = 0.009), but not in adult (t = 0.7, df = 12, p = 0.51) rats. The gray lines on C, H, -J, M, N, S-V indicate paired measurements.

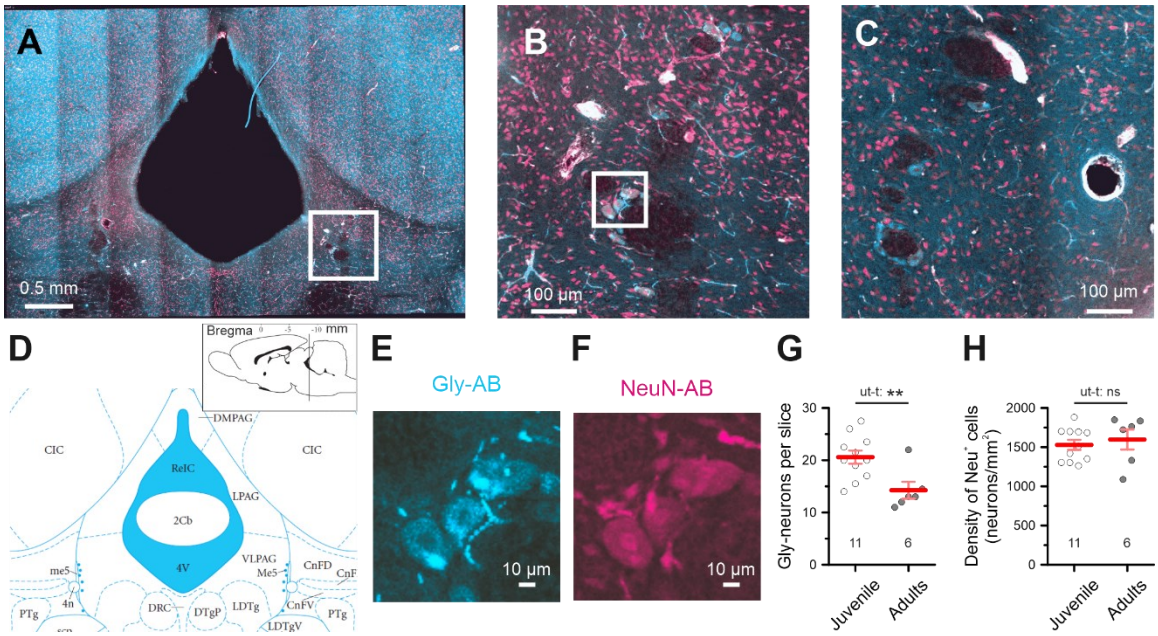

Figure S3. Glycinergic neurons in PAG slices. Related to Figure 3.

A. Confocal image of a coronal midbrain slice with PAG in the center, stained with antibodies to NeuN (red channel) and glycine (green channel). **B.** The enlarged portion of the caudal ventro-lateral PAG, marked with a white square in Figure A, represents a fragment of a brain slice from a juvenile rat. The white square highlights the localisation of glycinergic neurons. **C.** Fragment of caudal ventro-lateral PAG, from an adult rat brain slice corresponding to the area shown in Figure B. **D.** Schematic representation of the slice shown in Figure A, taken from the Paxinos atlas. **E-F.** Glycinergic neurons, highlighted by the white square in Figure B, stained with antibodies to glycine (**E**, green channel) and to NeuN (**F**, red channel). **G.** Comparison of the number of glycinergic neurons in the coronary brain slices of juvenile and adult rats. $t = 3.03$, $df = 15$, $p = 0.008$, Cohen's $d = 1.5$. **H.** The density of $NeuN^+$ neurons does not change significantly with age. $t = 0.54$, $df = 15$, $p = 0.6$, Cohen's $d = 0.27$. Abbreviations: DMPAG - dorsomedial PAG, LPAG - lateral PAG, VLPAG ventrolateral PAG, CIC - central nu. inferior colliculus, 4V - 4th ventricle, DRC - dorsal raphe nu. caudal part, DTgP - dorsal tegmental nu., LDTg - laterodorsal tegmental nu., Me5 - mesencephalic trigeminal tract., 4n - throchlear nerve.

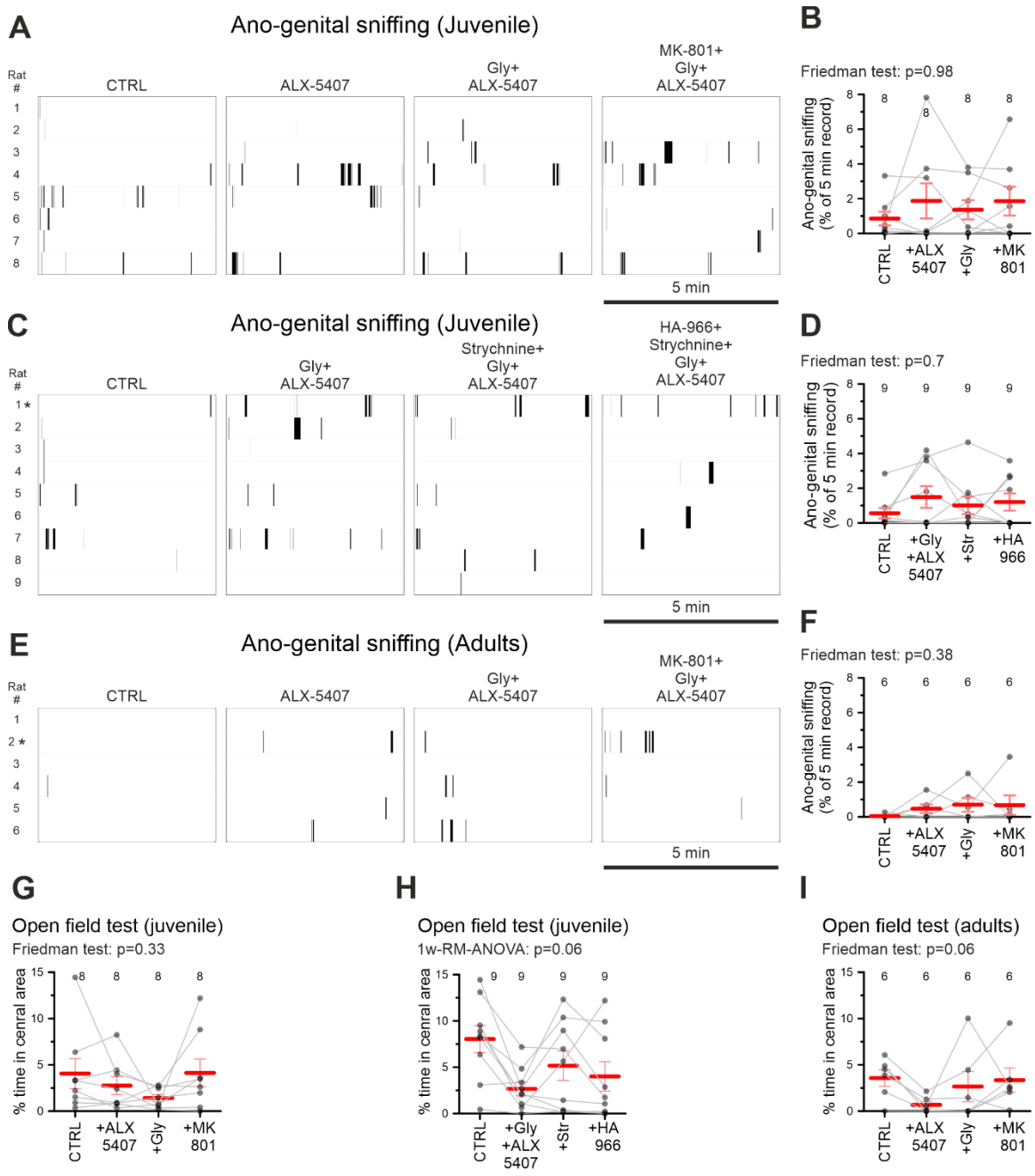

Figure S4. Glycine injected in PAG does not affect either social fear or anxiety. Related to Figure 4 and Figure 5.

A-F: Data for anogenital sniffing is non-playful social interactions inversely characterizing social fear. **A.** Timeline histograms of anogenital sniffing for juvenile rats after injections in PAG via guide cannulas of 0.9% NaCl control solution (CTRL), 2µM ALX-5407, GlyT1 blocker, a mixture of the previous substance with 100µM glycine

(Gly), and a mixture of all of the above with an NMDA receptor blocker, 10μM MK-801. The rats order is the same as on Figure 4A1. **B.** The statistics for the data in Figure A show that neither glycine nor NMDA receptors in PAG are responsible for anogenital sniffing, a non-playful social interaction. Friedman statistic = 0.2, p = 0.98. **C.** Timeline histograms of anogenital sniffing for juvenile rats after injections of control solution (CTRL), a mixture of 2μM ALX-5407 with 100μM glycine, a mixture of the previous substances with 2μM strychnine (Str), and a mixture of all of the above with 400μM HA-966, a blocker of Gly-binding site on NMDA receptor. The rats order is the same as on Figure 4B1. **D.** The statistics for the data in Figure C show that glycinergic receptors in PAG are not responsible for anogenitale sniffing. Friedman statistic = 1.4, p = 0.7. **E.** Timeline histograms of anogenital sniffing for adult rats after injections in PAG via guide cannulas of 0.9% NaCl control solution (CTRL), 2μM ALX-5407, GlyT1 blocker, a mixture of the previous substance with 100μM glycine (Gly), and a mixture of all of the above with an NMDA receptor blocker, 10μM MK-801. The rats order is the same as on Figure 5A. **F.** The statistics for the data in Figure A show that neither glycine nor NMDA receptors in PAG are responsible for anogenitale sniffing in adult rats. Friedman statistic = 3.4, p = 0.38. **G-I.** Statistics of the percentage of time animals spend in the central area in an open field test characterize anxiolytic effects. Note, ALX-5407 and Gly have an anxiogenic tendency. **G.** In the sequence of injections into the PAG of juvenile rats, the solutions 0.9% NaCl (CTRL), 2μM ALX-5407, a mixture of the previous substance with 100μM glycine (Gly), and a mixture of all of the above with 10μM MK-801 don't have significant anxiolytic effects. Friedman statistic = 3.5, p = 0.33. **H.** In the sequence of injections into the PAG of juvenile rats, the solutions 0.9% NaCl (CTRL), a mixture of 2μM ALX-5407 with 100μM glycine, a mixture of the previous substances with 2μM strychnine (Str) and a mixture of all of the above with 400μM HA-966 don't have significant anxiolytic effects. 1w-RM-ANOVA F (1.75, 13.97) = 3.7, p = 0.06. **I.** In the sequence of injections into the PAG of adult rats, the solutions 0.9% NaCl (CTRL), 2μM ALX-5407, a mixture of the previous substance with 100μM glycine (Gly), and a mixture of all of the above with 10μM MK-801 don't have significant anxiolytic effects. Friedman statistic = 7.4, p = 0.06.

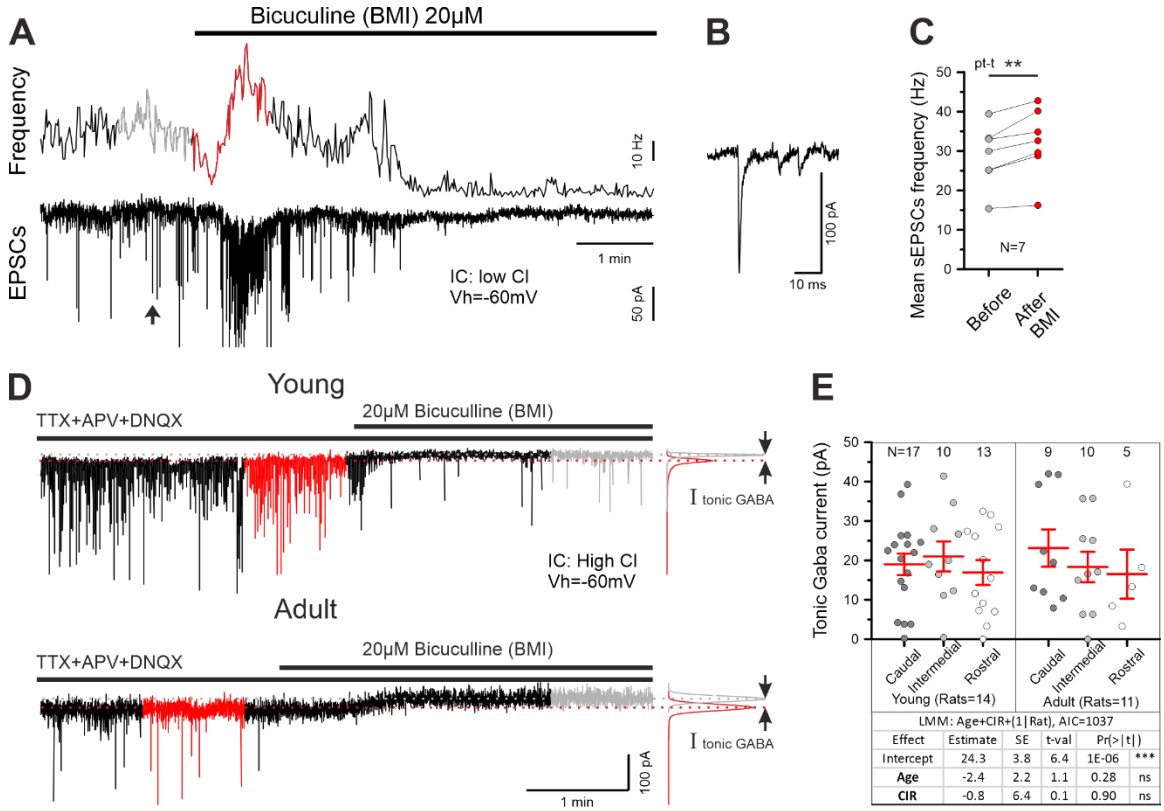

Figure S5. Tonic GABA currents increase inhibition in PAG slices regardless of age. Related to Figure 2.

A. Traces of sEPSCs (bottom trace) and their frequency (top trace) recorded with low Cl intrapipette solution (Vclrev = -60mV) at holding potential -60 mV in PAG neurons before and after application of 20μM bicuculline (BMI) show a temporal increase of sEPSCs frequency in the first minutes after BMI application. The arrow points to the enlarged fragment of the trace shown in figure **B.** The gray and red colors portions of the trace show the regions (1 min before (gray) and after (red) BMI application) used to calculate the mean sEPSCs frequency shown in figure **C** (Paired t-test: t=4.6, p=0.004). **D.** Example traces of mIPSCs recorded with high Cl intrapipette solution in the presence of 50μM APV + 10μM DNQX + 1μM TTX before and after additional application of 20μM bicuculline (BMI) in PAG neurons of juvenile (top trace) and adult (bottom trace) rats. The red (before BMI) and gray (after BMI) marked portions of the traces represent the regions used for the distribution diagrams shown on the right part of the figure. Note the upward shift of the baseline in presence of BMI defined as tonic GABA current. **E.** The statistics of tonic GABA currents measured in different PAG slices of juvenile and adult rats show no significant difference in these groups.

Comment	Parameters			Juvenile rats				Adult rats				Age-dependency				Effects directions	Correlation with playfulness in juvenile rats				
		Slice type	PAG column	Mean	SE	N	Norm. distr.	Mean	SE	N	Norm. distr.	% change	Cohen's d	p-value	Test	Age : Play corr.	r	Norm. distr.	p-value	N	Test
	Age at video shooting															: -	-0.232	No	0.2869	23	Spearman
	Age at in vitro experiment															: -	0.172	Yes	0.4329	23	Pearson
	Time of ano-genital contacts (%)															: -	0.052	Yes	0.8171	22	Pearson
Open field	Path length (m)															: -	-0.360	Yes	0.1554	17	Pearson
Open field	Mean velocity (mm/s)															: -	-0.211	No	0.4153	17	Spearman
Open field	Time of running (%)															: -	-0.066	Yes	0.8026	17	Pearson
Open field	Mean running velocity (mm/s)															: -	-0.147	No	0.5724	17	Spearman
Open field	The number of start/stop events															: -	-0.063	No	0.8115	17	Spearman
K+ IC solution	Max. frequency of action potentials (Hz)	Mixed	vlPAG	35.53	3.92	19	Yes	56.57	12.18	14	Yes			0.0735	ut-t	- :					
K+ IC solution	Reobase (pA)	Mixed	vlPAG	9.65	2.72	19	Yes	22.17	4.23	14	No	130	0.92	0.0235	MW	↑ :					
K+ IC solution	Half max. stimulation current, I50 (pA)	Mixed	vlPAG	71.13	9.46	19	Yes	94.79	20.87	14	No			0.6021	MW	- :					
K+ IC solution	Slope at I_{50} (Hz/pA)	Mixed	vlPAG	0.44	0.15	19	No	0.55	0.18	14	Yes			0.9857	MW	- :					
K+ IC solution	Frequency of action potentials (Hz)	Mixed	vlPAG	0.98	0.34	20	No	0.40	0.22	15	No	-59	0.45	0.0125	MW	↓ :					
K+ IC solution	Max. frequency of action potentials (Hz)	Mixed	dlPAG	59.58	10.62	19	No	63.50	17.15	12	Yes			0.8966	MW	- :					
K+ IC solution	Reobase (pA)	Mixed	dlPAG	10.57	7.34	19	No	35.71	7.97	11	No	238	0.83	0.0236	MW	↑ :					
K+ IC solution	Half max. stimulation current, I50 (pA)	Mixed	dlPAG	110.18	17.22	19	Yes	115.67	20.58	10	Yes			0.8464	ut-t	- :					
K+ IC solution	Slope at I_{50} (Hz/pA)	Mixed	dlPAG	0.40	0.06	19	No	0.51	0.14	10	Yes			0.9461	MW	- :					
K+ IC solution	Frequency of action potentials (Hz)	Mixed	dlPAG	2.09	0.64	27	No	0.76	0.47	12	No	-64	0.46	0.0493	MW	↓ :					
Cs+ IC solution	Tonic GABA-current (pA)	Caudal	dlPAG	19.00	2.74	17	Yes	23.13	4.71	9	Yes			0.4616	ut-t	- : ↑	0.618	No	0.0186	14	Spearman
Cs+ IC solution	Tonic GABA-current (pA)	Intermedial	dlPAG	21.00	3.81	10	Yes	18.34	3.86	10	Yes			0.6289	ut-t	- : -	0.506	Yes	0.2468	7	Pearson
Cs+ IC solution	Tonic GABA-current (pA)	Rostral	dlPAG	16.93	3.15	13	Yes	16.52	6.23	5	Yes			0.9550	ut-t	- : -	-0.134	Yes	0.7111	10	Pearson
Cs+ IC solution	Serial resistance (MOhm)	Caudal	dlPAG	10.92	0.44	63	No	11.32	0.84	15	Yes			0.5466	MW	- : ↓	-0.450	Yes	0.0312	23	Pearson
Cs+ IC solution	Serial resistance (MOhm)	Intermedial	dlPAG	10.33	0.38	64	Yes	11.32	0.37	30	Yes			0.0654	ut-t	- : -	0.104	No	0.6806	18	Spearman
Cs+ IC solution	Serial resistance (MOhm)	Rostral	dlPAG	11.12	0.60	38	No	11.09	0.56	25	Yes			0.5720	MW	- : -	-0.358	No	0.1585	17	Spearman
Cs+ IC solution	Membrane resistance (MOhm)	Caudal	dlPAG	523.56	30.70	63	No	372.78	48.75	15	Yes	-29	0.64	0.0246	MW	↓ : -	-0.224	No	0.3035	23	Spearman
Cs+ IC solution	Membrane resistance (MOhm)	Intermedial	dlPAG	409.34	23.59	64	No	470.67	40.52	30	No			0.2205	MW	- : -	0.154	Yes	0.5422	18	Pearson
Cs+ IC solution	Membrane resistance (MOhm)	Rostral	dlPAG	545.06	33.70	38	Yes	523.32	59.80	25	No			0.3528	MW	- : -	0.005	Yes	0.9846	17	Pearson
Cs+ IC solution	Input resistance (MOhm)	Caudal	dlPAG	534.48	30.82	63	No	384.10	49.18	15	Yes	-28	0.64	0.0254	MW	↓ : -	-0.229	No	0.2927	23	Spearman
Cs+ IC solution	Input resistance (MOhm)	Intermedial	dlPAG	419.67	23.77	64	No	481.99	40.64	30	No			0.2114	MW	- : -	0.155	Yes	0.5392	18	Pearson
Cs+ IC solution	Input resistance (MOhm)	Rostral	dlPAG	556.18	33.83	38	Yes	534.41	59.90	25	No			0.3601	MW	- : -	0.007	Yes	0.9781	17	Pearson
Cs+ IC solution	Membrane capacity (pF)	Caudal	dlPAG	46.03	3.54	63	No	50.12	8.48	15	No			0.5720	MW	- : -	0.132	Yes	0.5497	23	Pearson
Cs+ IC solution	Membrane capacity (pF)	Intermedial	dlPAG	57.46	3.69	64	Yes	39.69	4.27	30	Yes	-31	0.64	0.0024	ut-t	↓ : -	-0.090	Yes	0.7226	18	Pearson
Cs+ IC solution	Membrane capacity (pF)	Rostral	dlPAG	44.38	3.82	38	Yes	36.69	6.17	25	No	-17	0.29	0.0495	MW	↓ : -	0.040	Yes	0.8776	17	Pearson
Cs+ IC solution	sEPSC, Frequency (Hz)	Caudal	dlPAG	19.42	1.47	64	Yes	11.81	1.77	15	Yes	-39	0.69	0.0021	ut-t	↓ : -	0.182	Yes	0.4063	23	Pearson
Cs+ IC solution	sEPSC, Frequency (Hz)	Intermedial	dlPAG	22.46	1.64	64	No	11.21	1.16	30	Yes	-50	0.98	0.0000	MW	↓ : -	-0.376	Yes	0.1236	18	Pearson
Cs+ IC solution	sEPSC, Frequency (Hz)	Rostral	dlPAG	18.21	1.90	38	Yes	9.84	1.51	25	No	-46	0.81	0.0005	MW	↓ : -	0.101	Yes	0.7005	17	Pearson
Cs+ IC solution	sEPSC, Amplitude (pA)	Caudal	dlPAG	22.14	1.15	64	No	24.18	2.12	15	Yes			0.2609	MW	- : ↓	-0.561	No	0.0053	23	Spearman
Cs+ IC solution	sEPSC, Amplitude (pA)	Intermedial	dlPAG	26.97	1.35	64	Yes	22.21	1.12	30	Yes	-18	0.50	0.0081	ut-t	↓ : -	0.204	Yes	0.4165	18	Pearson
Cs+ IC solution	sEPSC, Amplitude (pA)	Rostral	dlPAG	21.14	1.02	38	Yes	23.89	1.74	25	Yes			0.1815	ut-t	- : -	-0.373	Yes	0.1403	17	Pearson
Cs+ IC solution	sEPSC, Baseline (pA)	Caudal	dlPAG	75.48	5.59	64	No	87.46	17.49	15	Yes			0.7998	MW	- : -	-0.067	No	0.7607	23	Spearman
Cs+ IC solution	sEPSC, Baseline (pA)	Intermedial	dlPAG	84.67	9.01	64	No	62.17	7.20	30	No			0.1059	MW	- : -	-0.098	No	0.6987	18	Spearman
Cs+ IC solution	sEPSC, Baseline (pA)	Rostral	dlPAG	70.44	8.22	38	No	74.52	7.80	25	Yes			0.3385	MW	- : -	-0.130	No	0.6192	17	Spearman
Cs+ IC solution	sEPSC, Integral (pA*ms)	Caudal	dlPAG	72.39	3.07	64	Yes	88.99	8.79	15	Yes			0.0918	ut-t	- : ↓	-0.510	No	0.0129	23	Spearman
Cs+ IC solution	sEPSC, Integral (pA*ms)	Intermedial	dlPAG	91.04	4.24	64	Yes	86.19	4.79	30	Yes			0.4515	ut-t	- : -	0.210	Yes	0.4033	18	Pearson
Cs+ IC solution	sEPSC, Integral (pA*ms)	Rostral	dlPAG	72.14	3.45	38	Yes	89.25	6.40	25	Yes	24	0.66	0.0239	ut-t	↑ : -	-0.346	Yes	0.1743	17	Pearson
Cs+ IC solution	sEPSC, Centroid (ms)	Caudal	dlPAG	1.75	0.06	64	Yes	2.20	0.13	15	Yes	26	0.95	0.0063	ut-t	↑ : -	0.190	Yes	0.3852	23	Pearson
Cs+ IC solution	sEPSC, Centroid (ms)	Intermedial	dlPAG	1.84	0.05	64	Yes	2.14	0.14	30	No	16	0.56	0.0006	MW	↑ : -	-0.102	Yes	0.6873	18	Pearson
Cs+ IC solution	sEPSC, Centroid (ms)	Rostral	dlPAG	1.87	0.09	38	Yes	2.36	0.09	25	Yes	26	0.92	0.0004	ut-t	↑ : -	-0.294	No	0.2518	17	Spearman
Cs+ IC solution	sEPSC, Rise time $_{20\text{-}90\%}$ (ms)	Caudal	dlPAG	0.91	0.01	64	Yes	0.90	0.01	15	Yes			0.6316	ut-t	- : -	0.233	Yes	0.2841	23	Pearson
Cs+ IC solution	sEPSC, Rise time $_{20\text{-}90\%}$ (ms)	Intermedial	dlPAG	0.91	0.01	64	Yes	0.93	0.02	30	Yes			0.5007	ut-t	- : -	-0.432	Yes	0.0733	18	Pearson
Cs+ IC solution	sEPSC, Rise time $_{20\text{-}90\%}$ (ms)	Rostral	dlPAG	0.92	0.02	38	Yes	0.89	0.01	25	Yes			0.2831	ut-t	- : -	0.053	Yes	0.8386	17	Pearson
Cs+ IC solution	sEPSC, Decay time to 50% (ms)	Caudal	dlPAG	1.10	0.03	64	No	1.15	0.06	15	Yes			0.4685	MW	- : -	0.164	Yes	0.4533	23	Pearson
Cs+ IC solution	sEPSC, Decay time to 50% (ms)	Intermedial	dlPAG	1.22	0.03	64	Yes	1.22	0.06	30	Yes			0.9683	ut-t	- : ↓	-0.573	Yes	0.0129	18	Pearson
Cs+ IC solution	sEPSC, Decay time to 50% (ms)	Rostral	dlPAG	1.13	0.04	38	Yes	1.13	0.05	25	Yes			0.9755	ut-t	- : -	0.042	Yes	0.8742	17	Pearson
Cs+ IC solution	sEPSC, Tau of monoexp. decay (ms)	Caudal	dlPAG	2.86	0.10	64	Yes	2.22	0.17	15	Yes	-22	0.85	0.0029	ut-t	↓ : -	-0.155	Yes	0.4791	23	Pearson
Cs+ IC solution	sEPSC, Tau of monoexp. decay (ms)	Intermedial	dlPAG	2.71	0.07	64	Yes	2.45	0.13	30	Yes			0.1009	ut-t	- : ↑	0.543	Yes	0.0199	18	Pearson
Cs+ IC solution	sEPSC, Tau of monoexp. decay (ms)	Rostral	dlPAG	2.91	0.15	38	Yes	2.07	0.10	25	Yes	-29	1.06	0.0000	ut-t	↓ : -	-0.034	No	0.8960	17	Spearman
Cs+ IC solution	sEPSC, Tau norm. to capacity (ms/pF)	Caudal	dlPAG	0.09	0.01	63	No	0.06	0.01	15	Yes	-32	0.55	0.0404	MW	↓ : -	-0.190	No	0.3859	23	Spearman
Cs+ IC solution	sEPSC, Tau norm. to capacity (ms/pF)	Intermedial	dlPAG	0.06	0.00	64	No	0.08	0.01	30	No	33	0.49	0.0204	MW	↑ : -	0.028	No	0.9126	18	Spearman
Cs+ IC solution	sEPSC, Tau norm. to capacity (ms/pF)	Rostral	dlPAG	0.09	0.01	38	No	0.08	0.01	25	No			0.9611	MW	- : -	0.221	Yes	0.3947	17	Pearson
Cs+ IC solution, TTX	mEPSC, Frequency (Hz)	Caudal	dlPAG	11.27	1.08	39	No	9.45	2.14	8	Yes			0.5877	MW	- : -	0.293	Yes	0.1744	23	Pearson
Cs+ IC solution, TTX	mEPSC, Frequency (Hz)	Intermedial	dlPAG	12.68	1.44	35	No	7.80	0.86	16	Yes	-39	0.67	0.0346	MW	↓ : -	-0.073	Yes	0.7815	17	Pearson
Cs+ IC solution, TTX	mEPSC, Frequency (Hz)	Rostral	dlPAG	8.72	0.91	21	Yes	7.29	1.70	10	Yes			0.4710	ut-t	- : -	-0.001	Yes	0.9960	15	Pearson
Cs+ IC solution, TTX	mEPSC, Amplitude (pA)	Caudal	dlPAG	16.13	0.63	39	Yes	24.64	3.92	8	Yes			0.0669	ut-t	- : ↓	-0.513	Yes	0.0123	23	Pearson
Cs+ IC solution, TTX	mEPSC, Amplitude (pA)	Intermedial	dlPAG	20.41	1.13	35	Yes	21.05	1.02	16	Yes			0.6786	ut-t	- : -	-0.147	Yes	0.5745	17	Pearson
Cs+ IC solution, TTX	mEPSC, Amplitude (pA)	Rostral	dlPAG	16.08	0.89	21	No	23.31	1.83	10	Yes	45	1.54	0.0003	MW	↑ : -	-0.070	Yes	0.8034	15	Pearson
Cs+ IC solution, TTX	mEPSC, Baseline (pA)	Caudal	dlPAG	106.13	11.59	39	No	224.53	77.65	8	Yes			0.3215	MW	- : -	-0.218	Yes	0.3174	23	Pearson
Cs+ IC solution, TTX	mEPSC, Baseline (pA)	Intermedial	dlPAG	182.32	37.24	35	No	123.64	20.04	16	No			0.6657	MW	- : -	0.265	No	0.3045	17	Spearman
Cs+ IC solution, TTX	mEPSC, Baseline (pA)	Rostral	dlPAG	165.33	44.84	21	No	103.84	22.22	10	No			0.5463	MW	- : -	0.293	Yes	0.2886	15	Pearson
Cs+ IC solution, TTX	mEPSC, Integral (pA*ms)	Caudal	dlPAG	55.78	3.04	39	Yes	88.83	13.97	8	Yes			0.0509	ut-t	- : ↓	-0.474	Yes	0.0225	23	Pearson
Cs+ IC solution, TTX	mEPSC, Integral (pA*ms)	Intermedial	dlPAG	73.38	4.32	35	Yes	80.15	3.15	16	Yes			0.2117	ut-t	- : -	-0.112	Yes	0.6685	17	Pearson
Cs+ IC solution, TTX	mEPSC, Integral (pA*ms)	Rostral	dlPAG	58.16	3.84	21	Yes	90.64	7.80	10	Yes	56	1.62	0.0023	ut-t	↑ : -	-0.111	Yes	0.6931	15	Pearson
Cs+ IC solution, TTX	mEPSC, Centroid (ms)	Caudal	dlPAG	1.66	0.15	39	No	2.37	0.14	8	Yes	42	0.80	0.0012	MW	↑ : -	0.188	No	0.3910	23	Spearman
Cs+ IC solution, TTX	mEPSC, Centroid (ms)	Intermedial	dlPAG	2.00	0.08	35	Yes	2.53	0.08	16	Yes	26	1.28	0.0000	ut-t	↑ : -	-0.390	Yes	0.1218	17	Pearson
Cs+ IC solution, TTX	mEPSC, Centroid (ms)	Rostral	dlPAG	1.96	0.10	21	Yes	2.59	0.09	10	Yes	32	1.54	0.0001	ut-t	↑ : -	-0.033	Yes	0.9074	15	Pearson
Cs+ IC solution, TTX	mEPSC, Rise time $_{20\text{-}90\%}$ (ms)	Caudal	dlPAG	0.86	0.02	39	Yes	0.84	0.01	8	Yes			0.4327	ut-t	- : -	0.271	Yes	0.2107	23	Pearson
Cs+ IC solution, TTX	mEPSC, Rise time $_{20\text{-}90\%}$ (ms)	Intermedial	dlPAG	0.89	0.01	35	Yes	0.89	0.01	16	Yes			0.8060	ut-t	- : -	-0.451	Yes	0.0694	17	Pearson
Cs+ IC solution, TTX	mEPSC, Rise time $_{20\text{-}90\%}$ (ms)	Rostral	dlPAG	0.89	0.03	21	Yes	0.90	0.02	10	Yes			0.8337	ut-t	- : -	0.093	Yes	0.7423	15	Pearson
Cs+ IC solution, TTX	mEPSC, Decay time to 50% (ms)	Caudal	dlPAG	0.97	0.05	39	Yes	1.08	0.06	8	Yes			0.1454	ut-t	- : ↑	0.431	Yes	0.0402	23	Pearson
Cs+ IC solution, TTX	mEPSC, Decay time to 50% (ms)	Intermedial	dlPAG	1.08	0.04	35	Yes	1.17	0.06	16	Yes			0.2221	ut-t	- : -	-0.003	Yes	0.9915	17	Pearson
Cs+ IC solution, TTX	mEPSC, Decay time to 50% (ms)	Rostral	dlPAG	0.96	0.05	21	Yes	1.14	0.05	10	No			0.0534	MW	- : -	0.091	Yes	0.7458	15	Pearson
Cs+ IC solution, TTX	mEPSC, Tau of monoexp. decay (ms)	Caudal	dlPAG	2.76	0.15	39	No	1.47	0.15	8	Yes	-47	1.47	0.0000	MW	↓ : -	-0.294	Yes	0.1736	23	Pearson
Cs+ IC solution, TTX	mEPSC, Tau of monoexp. decay (ms)	Intermedial	dlPAG	2.44	0.12	35	Yes	1.80	0.16	16	Yes	-26	0.95	0.0028	ut-t	↓ : -	0.282	Yes	0.2726	17	Pearson
Cs+ IC solution, TTX	mEPSC, Tau of monoexp. decay (ms)	Rostral	dlPAG	2.93	0.24	21	Yes	1.67	0.17	10	Yes	-43	1.32	0.0002	ut-t	↓ : -	-0.011	Yes	0.9680	15	Pearson
Cs+ IC solution, TTX	mEPSC, Tau norm. to capacity (ms/pF)	Caudal	dlPAG	0.08	0.01	38	No	0.04	0.01	8	Yes	-49	0.86	0.0122	MW	↓ : -	-0.136	Yes	0.5346	23	Pearson
Cs+ IC solution, TTX	mEPSC, Tau norm. to capacity (ms/pF)	Intermedial	dlPAG	0.05	0.01	35	No	0.07	0.01	16	Yes	32	0.42	0.0150	MW	↑ : -	-0.047	Yes	0.8575	17	Pearson
Cs+ IC solution, TTX	mEPSC, Tau norm. to capacity (ms/pF)	Rostral	dlPAG	0.08	0.01	21	No	0.06	0.01	10	Yes			0.3927	MW	- : -	0.265	Yes	0.3400	15	Pearson
Cs+ IC solution	% of TTX sensetive EPSCs	Caudal	dlPAG	39.62	2.88	33	Yes	10.85	3.06	8	No	-73	1.86	0.0000	MW	↓ : -	0.415	Yes	0.0615	21	Pearson
Cs+ IC solution	% of TTX sensetive EPSCs	Intermedial	dlPAG	38.28	3.69	33	Yes	23.17	2.76	16	Yes	-39	0.81	0.0020	ut-t	↓ : -	-0.084	Yes	0.7583	16	Pearson
Cs+ IC solution	% of TTX sensetive EPSCs	Rostral	dlPAG	43.57	4.52	21	Yes	37.65	5.61	10	Yes			0.4200	ut-t	- : -	-0.238	Yes	0.3921	15	Pearson
Cs+ IC solution	sIPSC, Frequency (Hz)	Caudal	dlPAG	26.66	2.20	59	Yes	18.36	3.70	11	Yes			0.0693	ut-t	- : -	0.267	Yes	0.2182	23	Pearson
Cs+ IC solution	sIPSC, Frequency (Hz)	Intermedial	dlPAG	28.22	2.47	51	No	15.58	2.04	22	No	-45	0.81	0.0043	MW	↓ : -	-0.449	Yes	0.0613	18	Pearson

Cs+ IC solution	sIPSC, Frequency (Hz)	Rostral	dlPAG	21.05	2.33	35	No	12.75	1.69	20	No	-39	0.70	0.0298	MW	↓ : -	0.159	Yes	0.5420	17	Pearson
Cs+ IC solution	sIPSC, Amplitude (pA)	Caudal	dlPAG	36.77	2.18	59	No	34.96	4.28	11	Yes			0.8486	MW	- : -	0.118	Yes	0.5905	23	Pearson
Cs+ IC solution	sIPSC, Amplitude (pA)	Intermedial	dlPAG	38.50	2.04	51	Yes	32.53	1.83	22	Yes	-15	0.46	0.0333	ut-t	↓ : ↓	-0.475	Yes	0.0463	18	Pearson
Cs+ IC solution	sIPSC, Amplitude (pA)	Rostral	dlPAG	30.82	1.25	35	Yes	38.46	3.96	20	No			0.0950	MW	- : -	-0.158	Yes	0.5440	17	Pearson
Cs+ IC solution	sIPSC, Baseline (pA)	Caudal	dlPAG	107.97	11.08	59	No	110.93	38.32	11	No			0.9422	MW	- : -	0.194	No	0.3759	23	Spearman
Cs+ IC solution	sIPSC, Baseline (pA)	Intermedial	dlPAG	115.34	12.52	51	Yes	82.40	9.83	22	Yes	-29	0.42	0.0422	ut-t	↓ : -	-0.307	Yes	0.2155	18	Pearson
Cs+ IC solution	sIPSC, Baseline (pA)	Rostral	dlPAG	70.84	11.90	35	No	55.57	7.25	20	No			0.2782	MW	- : -	0.328	No	0.1981	17	Spearman
Cs+ IC solution	sIPSC, Integral (pA*ms)	Caudal	dlPAG	175.83	7.59	59	Yes	189.26	27.43	11	Yes			0.6459	ut-t	- : -	0.034	Yes	0.8768	23	Pearson
Cs+ IC solution	sIPSC, Integral (pA*ms)	Intermedial	dlPAG	186.77	8.86	51	Yes	177.86	9.62	22	Yes			0.4987	ut-t	- : -	-0.365	Yes	0.1365	18	Pearson
Cs+ IC solution	sIPSC, Integral (pA*ms)	Rostral	dlPAG	164.30	10.57	35	No	223.45	19.83	20	Yes	36	0.81	0.0013	MW	↑ : -	-0.132	Yes	0.6135	17	Pearson
Cs+ IC solution	sIPSC, Centroid (ms)	Caudal	dlPAG	2.68	0.11	59	Yes	2.95	0.21	11	Yes			0.2762	ut-t	- : -	-0.300	Yes	0.1644	23	Pearson
Cs+ IC solution	sIPSC, Centroid (ms)	Intermedial	dlPAG	2.41	0.20	51	No	2.95	0.12	22	Yes	23	0.45	0.0219	MW	↑ : -	0.286	No	0.2502	18	Spearman
Cs+ IC solution	sIPSC, Centroid (ms)	Rostral	dlPAG	2.83	0.15	35	Yes	3.51	0.13	20	Yes	24	0.84	0.0014	ut-t	↑ : -	-0.001	Yes	0.9975	17	Pearson
Cs+ IC solution	sIPSC, Rise time $_{20\text{-}90\%}$ (ms)	Caudal	dlPAG	1.04	0.02	59	Yes	0.97	0.03	11	Yes	-7	0.65	0.0218	ut-t	↓ : -	0.013	Yes	0.9515	23	Pearson
Cs+ IC solution	sIPSC, Rise time $_{20\text{-}90\%}$ (ms)	Intermedial	dlPAG	1.04	0.02	51	Yes	1.03	0.02	22	Yes			0.8135	ut-t	- : -	0.263	No	0.2914	18	Spearman
Cs+ IC solution	sIPSC, Rise time $_{20\text{-}90\%}$ (ms)	Rostral	dlPAG	1.04	0.02	35	Yes	0.95	0.02	20	Yes	-9	0.73	0.0038	ut-t	↓ : -	0.449	Yes	0.0709	17	Pearson
Cs+ IC solution	sIPSC, Decay time to 50% (ms)	Caudal	dlPAG	2.18	0.06	59	Yes	1.94	0.13	11	Yes			0.1055	ut-t	- : -	0.129	Yes	0.5585	23	Pearson
Cs+ IC solution	sIPSC, Decay time to 50% (ms)	Intermedial	dlPAG	2.26	0.06	51	Yes	2.02	0.10	22	Yes			0.0560	ut-t	- : -	-0.192	Yes	0.4454	18	Pearson
Cs+ IC solution	sIPSC, Decay time to 50% (ms)	Rostral	dlPAG	2.17	0.09	35	Yes	2.15	0.12	20	Yes			0.8786	ut-t	- : -	0.105	Yes	0.6888	17	Pearson
Cs+ IC solution	sIPSC, Tau of monoexp. decay (ms)	Caudal	dlPAG	5.57	0.16	59	Yes	4.52	0.30	11	Yes	-19	0.87	0.0069	ut-t	↓ : -	-0.015	Yes	0.9473	23	Pearson
Cs+ IC solution	sIPSC, Tau of monoexp. decay (ms)	Intermedial	dlPAG	5.40	0.18	51	Yes	4.86	0.26	22	Yes			0.0942	ut-t	- : -	-0.086	No	0.7354	18	Spearman
Cs+ IC solution	sIPSC, Tau of monoexp. decay (ms)	Rostral	dlPAG	5.49	0.27	35	Yes	4.88	0.38	20	Yes			0.1993	ut-t	- : -	-0.135	No	0.6060	17	Spearman
Cs+ IC solution	sIPSC, Tau norm. to capacity (ms/pF)	Caudal	dlPAG	0.18	0.02	57	No	0.14	0.03	11	Yes			0.4197	MW	- : -	-0.329	Yes	0.1348	22	Pearson
Cs+ IC solution	sIPSC, Tau norm. to capacity (ms/pF)	Intermedial	dlPAG	0.14	0.02	50	No	0.18	0.03	22	No			0.2210	MW	- : -	0.343	Yes	0.1774	17	Pearson
Cs+ IC solution	sIPSC, Tau norm. to capacity (ms/pF)	Rostral	dlPAG	0.17	0.02	34	No	0.22	0.04	20	No			0.1505	MW	- : ↑	0.529	No	0.0350	16	Spearman
Cs+ IC solution, TTX	mIPSC, Frequency (Hz)	Caudal	dlPAG	14.15	1.70	35	Yes	8.14	1.66	7	Yes	-42	0.64	0.0194	ut-t	↓ : ↑	0.691	No	0.0005	21	Spearman
Cs+ IC solution, TTX	mIPSC, Frequency (Hz)	Intermedial	dlPAG	16.47	2.62	34	No	11.11	2.04	15	No			0.3168	MW	- : -	-0.144	Yes	0.6089	15	Pearson
Cs+ IC solution, TTX	mIPSC, Frequency (Hz)	Rostral	dlPAG	11.65	2.11	21	No	9.59	2.06	12	No			0.7191	MW	- : -	0.348	Yes	0.2032	15	Pearson
Cs+ IC solution, TTX	mIPSC, Amplitudes (pA)	Caudal	dlPAG	28.45	1.89	35	Yes	26.60	2.65	7	Yes			0.5798	ut-t	- : -	0.200	Yes	0.3852	21	Pearson
Cs+ IC solution, TTX	mIPSC, Amplitudes (pA)	Intermedial	dlPAG	33.29	2.73	34	Yes	32.25	2.67	15	Yes			0.7874	ut-t	- : -	-0.311	No	0.2597	15	Spearman
Cs+ IC solution, TTX	mIPSC, Amplitudes (pA)	Rostral	dlPAG	29.18	2.31	21	Yes	35.76	4.53	12	No			0.1411	MW	- : -	0.040	Yes	0.8870	15	Pearson
Cs+ IC solution, TTX	mIPSC, Bases (pA)	Caudal	dlPAG	92.40	9.16	35	Yes	91.07	29.85	7	Yes			0.9673	ut-t	- : ↑	0.497	Yes	0.0218	21	Pearson
Cs+ IC solution, TTX	mIPSC, Bases (pA)	Intermedial	dlPAG	128.76	16.68	34	No	86.78	15.81	15	Yes			0.3837	MW	- : -	-0.099	Yes	0.7256	15	Pearson
Cs+ IC solution, TTX	mIPSC, Bases (pA)	Rostral	dlPAG	74.40	12.26	21	Yes	56.01	14.51	12	Yes			0.3420	ut-t	- : -	0.093	Yes	0.7418	15	Pearson
Cs+ IC solution, TTX	mIPSC, Integral (pA*ms)	Caudal	dlPAG	174.69	11.35	35	Yes	137.85	18.75	7	Yes			0.1209	ut-t	- : -	0.099	Yes	0.6689	21	Pearson
Cs+ IC solution, TTX	mIPSC, Integral (pA*ms)	Intermedial	dlPAG	182.71	15.53	34	No	190.57	16.27	15	Yes			0.7287	MW	- : -	-0.511	No	0.0517	15	Spearman
Cs+ IC solution, TTX	mIPSC, Integral (pA*ms)	Rostral	dlPAG	183.98	14.84	21	Yes	206.91	28.20	12	Yes			0.4815	ut-t	- : -	-0.206	Yes	0.4615	15	Pearson
Cs+ IC solution, TTX	mIPSC, Centroid (ms)	Caudal	dlPAG	3.51	0.20	35	No	3.22	0.24	7	Yes			0.8173	MW	- : -	-0.168	Yes	0.4674	21	Pearson
Cs+ IC solution, TTX	mIPSC, Centroid (ms)	Intermedial	dlPAG	3.06	0.15	34	Yes	3.36	0.20	15	Yes			0.2472	ut-t	- : -	-0.226	Yes	0.4177	15	Pearson
Cs+ IC solution, TTX	mIPSC, Centroid (ms)	Rostral	dlPAG	3.63	0.24	21	No	3.37	0.20	12	Yes			0.4217	MW	- : -	-0.350	No	0.2009	15	Spearman
Cs+ IC solution, TTX	mIPSC, Rise time $_{20\text{-}90\%}$ (ms)	Caudal	dlPAG	1.09	0.04	35	No	0.91	0.03	7	Yes	-17	0.96	0.0063	MW	↓ : -	0.319	No	0.1580	21	Spearman
Cs+ IC solution, TTX	mIPSC, Rise time $_{20\text{-}90\%}$ (ms)	Intermedial	dlPAG	1.03	0.03	34	Yes	1.01	0.03	15	No			0.9061	MW	- : -	-0.439	No	0.1014	15	Spearman
Cs+ IC solution, TTX	mIPSC, Rise time $_{20\text{-}90\%}$ (ms)	Rostral	dlPAG	1.09	0.05	21	No	0.93	0.02	12	Yes	-15	0.86	0.0330	MW	↓ : -	-0.135	Yes	0.6305	15	Pearson
Cs+ IC solution, TTX	mIPSC, Decay time to 50% (ms)	Caudal	dlPAG	2.39	0.14	35	Yes	1.54	0.15	7	Yes	-36	1.10	0.0007	ut-t	↓ : -	0.351	Yes	0.1188	21	Pearson
Cs+ IC solution, TTX	mIPSC, Decay time to 50% (ms)	Intermedial	dlPAG	2.18	0.12	34	Yes	2.15	0.18	15	Yes			0.8913	ut-t	- : ↓	-0.605	Yes	0.0169	15	Pearson
Cs+ IC solution, TTX	mIPSC, Decay time to 50% (ms)	Rostral	dlPAG	2.34	0.17	21	Yes	2.00	0.18	12	Yes			0.1766	ut-t	- : -	0.041	Yes	0.8855	15	Pearson
Cs+ IC solution, TTX	mIPSC, Tau of monoexp. decay (ms)	Caudal	dlPAG	6.54	0.39	35	Yes	2.97	0.51	7	Yes	-55	1.62	0.0001	ut-t	↓ : -	-0.199	Yes	0.3881	21	Pearson
Cs+ IC solution, TTX	mIPSC, Tau of monoexp. decay (ms)	Intermedial	dlPAG	5.38	0.32	34	Yes	4.55	0.42	15	Yes			0.1213	ut-t	- : -	0.487	Yes	0.0655	15	Pearson
Cs+ IC solution, TTX	mIPSC, Tau of monoexp. decay (ms)	Rostral	dlPAG	6.45	0.46	21	Yes	3.92	0.40	12	Yes	-39	1.35	0.0002	ut-t	↓ : -	0.038	Yes	0.8920	15	Pearson
Cs+ IC solution, TTX	mIPSC, Tau norm. to capacity (ms/pF)	Caudal	dlPAG	0.21	0.03	35	No	0.09	0.03	7	Yes			0.0791	MW	- : -	-0.251	No	0.2731	21	Spearman
Cs+ IC solution, TTX	mIPSC, Tau norm. to capacity (ms/pF)	Intermedial	dlPAG	0.11	0.01	33	No	0.18	0.03	15	No			0.0819	MW	- : -	0.187	Yes	0.5221	14	Pearson
Cs+ IC solution, TTX	mIPSC, Tau norm. to capacity (ms/pF)	Rostral	dlPAG	0.18	0.03	20	No	0.15	0.03	12	Yes			0.5778	MW	- : -	0.371	Yes	0.1918	14	Pearson
Cs+ IC solution	% of TTX sensetive IPSCs	Caudal	dlPAG	41.97	3.51	28	Yes	30.13	7.57	6	Yes			0.1971	ut-t	- : -	-0.402	Yes	0.0708	21	Pearson
Cs+ IC solution	% of TTX sensetive IPSCs	Intermedial	dlPAG	38.66	4.82	23	No	25.21	5.26	12	Yes			0.1723	MW	- : -	0.312	Yes	0.2779	14	Pearson
Cs+ IC solution	% of TTX sensetive IPSCs	Rostral	dlPAG	45.53	5.82	19	Yes	29.09	4.63	11	Yes	-36	0.74	0.0354	ut-t	↓ : -	-0.492	Yes	0.0742	14	Pearson
Cs+ IC solution	E/I (%)	Caudal	dlPAG	85.22	5.43	54	Yes	66.63	8.57	11	Yes			0.0826	ut-t	- : -	-0.174	No	0.4274	23	Spearman
Cs+ IC solution	E/I (%)	Intermedial	dlPAG	94.06	5.58	47	Yes	76.69	6.53	22	Yes	-18	0.48	0.0485	ut-t	↓ : -	0.443	No	0.0658	18	Spearman
Cs+ IC solution	E/I (%)	Rostral	dlPAG	110.58	9.72	33	No	81.88	5.63	20	Yes	-26	0.61	0.0317	MW	↓ : -	0.060	Yes	0.8179	17	Pearson
Cs+ IC solution, TTX	E/I in presence of TTX(%)	Caudal	dlPAG	98.93	12.13	32	No	112.82	19.17	6	Yes			0.4448	MW	- : -	-0.304	No	0.1805	21	Spearman
Cs+ IC solution, TTX	E/I in presence of TTX(%)	Intermedial	dlPAG	106.72	11.75	31	No	88.00	8.61	15	Yes			0.7282	MW	- : -	0.464	No	0.0813	15	Spearman
Cs+ IC solution, TTX	E/I in presence of TTX(%)	Rostral	dlPAG	101.72	14.56	16	Yes	77.05	7.78	10	Yes			0.1492	ut-t	- : -	-0.222	No	0.4456	14	Spearman
Cs+ IC solution	TTX effect for E/I (%)	Caudal	dlPAG	6.96	8.94	23	Yes	58.26	25.84	5	Yes			0.1195	ut-t	- : ↓	-0.448	Yes	0.0477	20	Pearson
Cs+ IC solution	TTX effect for E/I (%)	Intermedial	dlPAG	0.75	11.23	18	Yes	12.35	12.42	12	Yes			0.4950	ut-t	- : -	0.235	No	0.4183	14	Spearman
Cs+ IC solution	TTX effect for E/I (%)	Rostral	dlPAG	10.66	11.37	15	Yes	4.75	8.14	9	Yes			0.2823	ut-t	- : -	-0.393	No	0.1640	14	Spearman
Cs+ IC solution, TTX, BMI	Gly-mIPSC, Frequency (Hz)	Caudal	dlPAG	1.31	0.26	30	No	0.37	0.21	16	No	-72	0.76	0.0063		↓ : ↑	0.604	No	0.0062	19	Spearman
Cs+ IC solution, TTX, BMI	Gly-mIPSC, Frequency (Hz)	Intermedial	dlPAG	1.50	0.37	15	Yes	0.16	0.08	9	No	-89	1.16	0.0029		↓ : -	0.088	Yes	0.7967	11	Pearson
Cs+ IC solution, TTX, BMI	Gly-mIPSC, Frequency (Hz)	Rostral	dlPAG	0.62	0.16	18	Yes	0.01	0.00	5	No	-98	1.03	0.0011		↓ : -	-0.079	No	0.7808	15	Spearman
Cs+ IC solution, TTX, BMI	Gly-mIPSC, Amplitudes (pA)	Caudal	dlPAG	16.17	0.76	30	Yes	16.26	1.54	13	Yes			0.9592		- : -	0.167	No	0.4953	19	Spearman
Cs+ IC solution, TTX, BMI	Gly-mIPSC, Amplitudes (pA)	Intermedial	dlPAG	17.49	1.30	15	Yes	20.06	5.04	7	Yes			0.6364		- : -	-0.082	Yes	0.8098	11	Pearson
Cs+ IC solution, TTX, BMI	Gly-mIPSC, Amplitudes (pA)	Rostral	dlPAG	15.79	1.08	18	Yes	16.75		1						: -	0.032	No	0.9095	15	Spearman
Cs+ IC solution, TTX, BMI	Gly-mIPSC, Bases (pA)	Caudal	dlPAG	50.34	8.35	27	Yes	32.92	9.04	11	Yes			0.1684		- : ↑	0.605	Yes	0.0061	19	Pearson
Cs+ IC solution, TTX, BMI	Gly-mIPSC, Bases (pA)	Intermedial	dlPAG	92.37	19.18	11	Yes	12.35	17.11	5	Yes	-87	1.39	0.0086		↓ : -	0.219	Yes	0.5171	11	Pearson
Cs+ IC solution, TTX, BMI	Gly-mIPSC, Bases (pA)	Rostral	dlPAG	56.13	10.32	15	Yes									: -	-0.046	Yes	0.8721	15	Pearson
Cs+ IC solution, TTX, BMI	Gly-mIPSC, Integral (pA*ms)	Caudal	dlPAG	92.13	11.32	27	No	78.9247	17.72	11	No			0.5376		- : -	0.118	No	0.6318	19	Spearman
Cs+ IC solution, TTX, BMI	Gly-mIPSC, Integral (pA*ms)	Intermedial	dlPAG	94.03	21.20	11	Yes	38.8044	9.999	4	0	-59	0.88	0.0351		↓ : -	-0.201	Yes	0.5543	11	Pearson
Cs+ IC solution, TTX, BMI	Gly-mIPSC, Integral (pA*ms)	Rostral	dlPAG	218.68	92.72	15	No									: -	0.211	No	0.4510	15	Spearman
Cs+ IC solution, TTX, BMI	Gly-mIPSC, Centroid (ms)	Caudal	dlPAG	3.10	0.40	27	No	2.81734	0.29	11	Yes			0.5764		- : -	-0.124	Yes	0.6118	19	Pearson
Cs+ IC solution, TTX, BMI	Gly-mIPSC, Centroid (ms)	Intermedial	dlPAG	2.59	0.36	11	Yes	1.73491	0.4308	4	0			0.1693		- : -	-0.357	Yes	0.2810	11	Pearson
Cs+ IC solution, TTX, BMI	Gly-mIPSC, Centroid (ms)	Rostral	dlPAG	4.15	0.76	15	Yes									: -	0.086	No	0.7613	15	Spearman
Cs+ IC solution, TTX, BMI	Gly-mIPSC, Rise time $_{20\text{-}90\%}$ (ms)	Caudal	dlPAG	0.97	0.07	30	Yes	0.84993	0.0847	13	Yes			0.274		- : -	0.122	Yes	0.6175	19	Pearson
Cs+ IC solution, TTX, BMI	Gly-mIPSC, Rise time $_{20\text{-}90\%}$ (ms)	Intermedial	dlPAG	0.82	0.09	15	Yes	0.76367	0.1347	7	Yes			0.7487		- : -	-0.405	Yes	0.2164	11	Pearson
Cs+ IC solution, TTX, BMI	Gly-mIPSC, Rise time $_{20\text{-}90\%}$ (ms)	Rostral	dlPAG	0.97	0.10	18	Yes	0.995								: -	-0.259	Yes	0.3506	15	Pearson
Cs+ IC solution, TTX, BMI	Gly-mIPSC, Decay time to 50% (ms)	Caudal	dlPAG	1.33	0.18	30	No	1.37873	0.2894	13	Yes			0.8949		- : -	0.002	Yes	0.9931	19	Pearson
Cs+ IC solution, TTX, BMI	Gly-mIPSC, Decay time to 50% (ms)	Intermedial	dlPAG	1.66	0.30	15	Yes	1.9966	0.7373	7	Yes			0.679		- : -	-0.266	Yes	0.4299	11	Pearson
Cs+ IC solution, TTX, BMI	Gly-mIPSC, Decay time to 50% (ms)	Rostral	dlPAG	2.21	0.43	18	No	5.30667								: -	0.325	Yes	0.2367	15	Pearson
Cs+ IC solution, TTX, BMI	Gly-mIPSC, Tau of monoexp. decay (ms)	Caudal	dlPAG	4.75	0.49	30	Yes	4.49104	0.7849	10	Yes			0.7824		- : -	-0.024	Yes	0.9229	19	Pearson
Cs+ IC solution, TTX, BMI	Gly-mIPSC, Tau of monoexp. decay (ms)	Intermedial	dlPAG	4.40	0.73	15	Yes	2.82868	0.6423	5	Yes			0.1276		- : -	0.407	Yes	0.2138	11	Pearson
Cs+ IC solution, TTX, BMI	Gly-mIPSC, Tau of monoexp. decay (ms)	Rostral	dlPAG	5.99	1.21	18	Yes	5.09823								: -	-0.285	Yes	0.3027	15	Pearson
Cs+ IC solution, TTX, BMI	Gly-mIPSC, Tau norm. to capacity (ms/pF)	Caudal	dlPAG	0.15	0.03	27	No	0.27403	0.1343	8	No			0.4074		- : -	-0.167	No	0.4953	19	Spearman
Cs+ IC solution, TTX, BMI	Gly-mIPSC, Tau norm. to capacity (ms/pF)	Intermedial	dlPAG	0.10	0.02	11	Yes	0.07905	0.0361	3				0.6626		- : -	-0.248	Yes	0.4621	11	Pearson
Cs+ IC solution, TTX, BMI	Gly-mIPSC, Tau norm. to capacity (ms/pF)	Rostral	dlPAG	0.18	0.04	15	Yes									: -	0.352	Yes	0.1981	15	Pearson
Cs+ IC solution	Frequency of BMI sensetive mIPSCs (Hz)	Caudal	dlPAG													: -	-0.043	Yes	0.8610	19	Pearson
Cs+ IC solution	Frequency of BMI sensetive mIPSCs (Hz)	Intermedial	dlPAG													: -	-0.065	Yes	0.8500	11	Pearson
Cs+ IC solution	Frequency of BMI sensetive mIPSCs (Hz)	Rostral	dlPAG													: -	0.209	No	0.4738	14	Spearman

Table S1. Age dependency of electrophysiologic parameters in PAG slices and their correlation with playfulness. Related to Figure 2.